



HAL
open science

The role of serpentization and magmatism in the formation of decoupling interfaces at magma-poor rifted margins

Morgane Gillard, Julie Tugend, Othmar Müntener, Gianreto Manatschal, Garry D. Karner, Julia Autin, Daniel Sauter, Patricio H Figueredo, Marc Ulrich

► To cite this version:

Morgane Gillard, Julie Tugend, Othmar Müntener, Gianreto Manatschal, Garry D. Karner, et al.. The role of serpentization and magmatism in the formation of decoupling interfaces at magma-poor rifted margins. *Earth-Science Reviews*, 2019, 196, pp.102882. 10.1016/j.earscirev.2019.102882 . hal-02308584

HAL Id: hal-02308584

<https://hal.sorbonne-universite.fr/hal-02308584>

Submitted on 8 Oct 2019

HAL is a multi-disciplinary open access archive for the deposit and dissemination of scientific research documents, whether they are published or not. The documents may come from teaching and research institutions in France or abroad, or from public or private research centers.

L'archive ouverte pluridisciplinaire **HAL**, est destinée au dépôt et à la diffusion de documents scientifiques de niveau recherche, publiés ou non, émanant des établissements d'enseignement et de recherche français ou étrangers, des laboratoires publics ou privés.

1 The role of serpentinization and magmatism in the formation of decoupling 2 interfaces at magma-poor rifted margins

3

4 Morgane Gillard^{*a1}, Julie Tugend^{a,b,c}, Othmar Müntener^d, Gianreto Manatschal^a, Garry D. Karner^e, Julia
5 Autin^a, Daniel Sauter^a, Patricio H. Figueredo^e, Marc Ulrich^a

6 *Corresponding author: Morgane Gillard (morgane.gillard@upmc.fr)

7

8 (a) Institut de Physique du Globe de Strasbourg, UMR7516, Université de Strasbourg/EOST, CNRS, 1 rue Blessig,
9 Strasbourg, Cedex, F-67084, France

10 (b) Sorbonne Université, CNRS-INSU, Institut des Sciences de la Terre Paris, ITeP UMR 7193, F-75005 Paris, France

11 (c) Total SA, R&D department CSTJF, Pau, France

12 (d) Institute of Earth Sciences, University of Lausanne, Géopolis, CH-1015 Lausanne, Switzerland.

13 (e) ExxonMobil Upstream Integrated Solutions Company, Global Tectonics & Structure, 22777 Springwoods Village
14 Parkway, Spring, Texas, USA

15 (1) Present address: Sorbonne Université, CNRS-INSU, Institut des Sciences de la Terre Paris, ITeP UMR 7193, F-
16 75005 Paris, France

17

18 Declarations of interest: none

19

20 Abstract

21 In spite of recent progress in the understanding of magma-poor rifted margins, the processes leading to
22 the formation and evolution of the exhumed mantle domain and its transition toward steady state oceanic
23 crust remain debated. In particular, the parameters controlling the progressive localization of extensional
24 deformation and magmatic processes leading to the formation of an oceanic spreading center are poorly
25 understood. In this paper, we highlight the occurrence of two major decoupling horizons controlling the
26 structural and magmatic evolution of distal magma-poor rifted margins. They are marked by strong seismic
27 reflectors located at about 1 sec TWTT (Upper Reflectors–UR) and 2 sec TWTT (Lower Reflectors–LR) below
28 top basement in domains of exhumed mantle at several magma-poor rifted margins. Both reflection
29 seismic observations and studies on the physical properties of serpentinized mantle suggest that the UR

30 likely results from deformation localized along a rheological interface at about 3 km below top basement,
31 associated with an abrupt change in the mechanical behavior of peridotites once they are serpentinized
32 to ~15%. We suggest that this interface played a major role in successive fault re-organizations during
33 formation of the exhumed mantle domain. The comparison of reflection seismic observations with Alpine
34 field analogues suggests that the LR likely results from an interaction between magmatism, deformation
35 and hydration reactions during final rifting. Based on our results, we suggest that during final rifting the
36 strain distribution is controlled first by hydration and then by magmatic processes in the domain of
37 exhumed mantle.

38

39 Keywords: Serpentinization; Magma-poor margins; Decoupling; Seismic interpretation

40

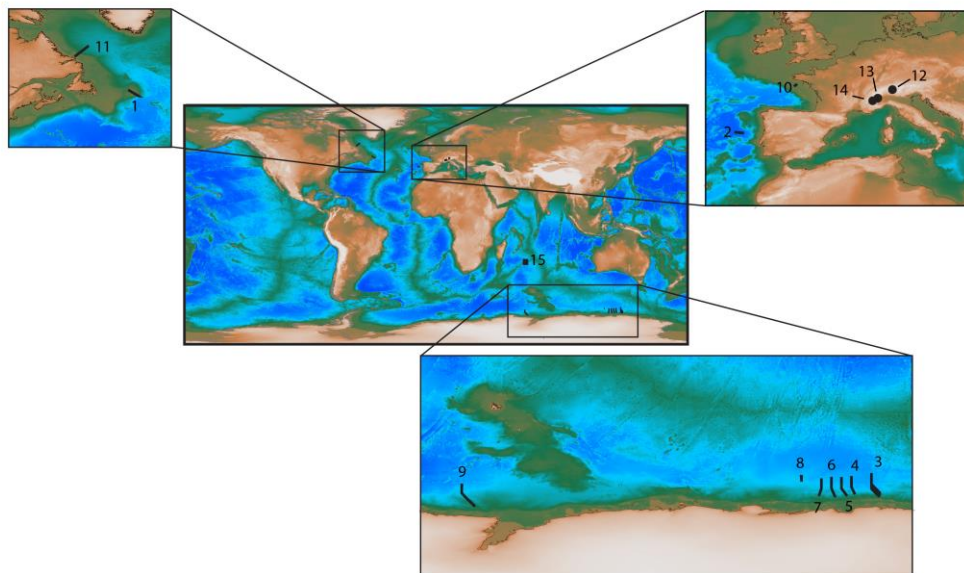
41 **1. Introduction and scientific context**

42 Major progress has been made in understanding the architecture of magma-poor rifted margins
43 (e.g., Peron-Pinvidic et al., 2013; Reston, 2009). At present, it is generally accepted that the transition zone
44 located between the edge of continental and first unambiguous oceanic crusts, also referred to as the
45 Ocean Continent Transition (OCT), can include a zone of exhumed subcontinental serpentinized mantle.
46 The presence of such a basement type is attested at several distal rifted margins based on drilling (e.g.
47 Iberia-Newfoundland (Boillot et al., 1988; Sawyer et al., 1994; Whitmarsh et al., 1998; Tucholke et al.,
48 2004); Tyrrhenian Sea (Bonatti et al., 1990)) and dredges (e.g. Australia-Antarctica (Beslier et al., 2004)).
49 This is further supported by reflection and refraction seismic data (e.g. southern North Atlantic margins
50 (Reston, 2007; Minshull, 2009)), or potential field data (e.g. SE-India (Nemcok et al., 2013); Bay of Biscay
51 (Thinon et al., 2003; Tugend et al., 2014)). However, how this zone of exhumed mantle forms and evolves

52 to steady state oceanic spreading remains an open question, notably, how extensional deformation
53 interacts with serpentinization and onset of magmatic activity.

54 Evidence for polyphase deformation and an interaction with serpentinization and magmatic
55 processes is inferred both from field observations and reflection seismic data (Desmurs et al., 2001, 2002;
56 Picazo et al., 2016; Gillard et al., 2015). The organization and geometry of fault systems in exhumed mantle
57 domains appear polyphase, showing in-sequence and/or out-of-sequence stepping of faults resulting in a
58 complex final basement architecture (Reston and McDermott, 2011; Gillard et al., 2016a). However, the
59 processes that control the stepping and evolution of these faults remain poorly constrained, as are the
60 way high-angle normal faults interact with extensional detachment systems (exhumation faults) and the
61 nature and depth of their decoupling levels (Boillot and Froitzheim, 2001; Reston and McDermott, 2011;
62 Gillard et al., 2016b). On reflection seismic sections, normal faults often seem to interact with intra-
63 basement decoupling interfaces that generally appear as strong reflections. A well-studied example is the
64 S-reflector, located at the base of hyperextended continental crust of the Galicia rifted margin (Sibuet,
65 1992; Reston, 1996; Whitmarsh et al., 1996; Reston and Pérez-Gussinyé, 2007; Reston, 2009; Lymer et al.
66 2019). The S-reflector is commonly interpreted as a decollement due to the presence of a sole of
67 serpentinized mantle, suggesting that hydration processes can control the structural evolution of
68 hyperextended and exhumed mantle domains (Pérez-Gussinyé and Reston, 2001; Pérez-Gussinyé et al.,
69 2001; Bayrakci et al., 2016). Other intra-basement reflectors have also been identified in more distal
70 domains of magma-poor rifted margins, for example the Z reflection at the Newfoundland margin (Hopper
71 et al., 2006) or the D reflection at the Labrador margins (Chian et al., 1995), which are localized in domains
72 of exhumed mantle. In these newly formed domains, both serpentinization and magmatism control the
73 composition, thermal state and rheology of the basement. Consequently, the nature and origin of these
74 intra-basement reflections and the evolution and localization of deformation in these ultra-distal domains
75 remain unclear.

76 The aim of this study is twofold. First, we describe different types of coherent seismic reflectors that
77 may have acted as decoupling interfaces in exhumed mantle domains, using several examples of magma-
78 poor rifted margins (Fig. 1). We describe their geometry, position and their geometrical relationship to
79 fault structures. In a second part, we discuss the potential mechanisms related to their formation based
80 on a multi-disciplinary approach and we explore the influence of hydrothermal circulation,
81 serpentinization and magmatism on the structural evolution of ultra-distal domains at magma-poor rifted
82 margins.



83
84 **Figure 1: Location map of the different seismic profiles and field analogues described in this study. 1: Screech1 (Newfoundland**
85 **margin); 2: IAM9 (Iberian margin); 3: GA228-27 (Antarctica margin); 4: GA228-25 (Antarctica margin); 5: GA228-24 (Antarctica**
86 **margin); 6: GA228-23 (Antarctica margin); 7: GA228-22 (Antarctica margin); 8: GA229-10 (Antarctica margin); 9: GA228-06**
87 **(Antarctica margin); 10: Norgasis23 (Bay of Biscay); 11: Line3 (Labrador margin); 12: Platta nappe (fossil analogue, Alps); 13:**
88 **Lanzo Massif (fossil analogue, Alps); 14: Chenaillet ophiolite (fossil analogue, Alps); 15: Axial valley of the Southwest Indian**
89 **Ridge (present day analogue).**

90 The results of our study provide a conceptual understanding of how serpentinization and
91 magmatism may control strain distribution during mantle exhumation at distal margins and enable us to

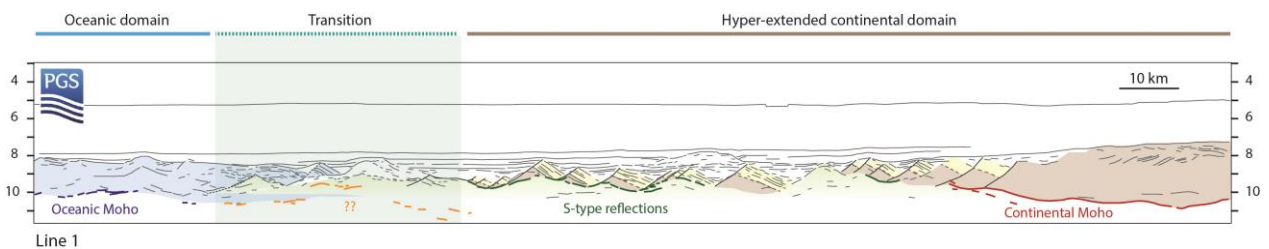
92 discuss the processes controlling the polyphase evolution of these domains. Unravelling the nature and
93 significance of these intra-basement reflectors and their potential role as decoupling interfaces provides
94 new insights into the processes controlling the transition from exhumation of subcontinental mantle to
95 oceanic spreading.

96

97 2. Seismic observations: intra-basement reflections

98 In this section, we identify and characterize potential decoupling interfaces at Ocean Continent
99 Transitions of magma-poor rifted margins. The studied areas are thus located between the edge of
100 unambiguous continental and first oceanic crusts (Fig. 2). In this study we do neither investigate
101 continental nor oceanic Mohos, nor the S-type reflections (localized landward of the continental crust
102 termination) (Fig. 2). Except for the Iberia-Newfoundland rifted margins and the Tyrrhenian Sea where
103 serpentinized peridotites have been drilled (Boillot et al., 1988; Bonatti et al., 1990; Sawyer et al., 1994;
104 Whitmarsh et al., 1998; Tucholke et al., 2004), interpretation of basement nature in distal domains relies
105 on reflection, refraction seismic data and/or potential field data, leading to a variety of propositions.

106



107 **Figure 2: Seismic line drawing illustrating the main reflections that can be observed at magma-poor rifted margins and their**
108 **locations. The area studied in this paper is highlighted in light green. Figure modified from Gillard et al. 2017. Seismic line**
109 **located in the Gulf of Guinea.**

110 On reflection seismic sections, the exhumed mantle domain is generally characterized by the absence
111 of “pre-exhumation” (generally considered as “pre-rift”) sediments (exceptions are extensional

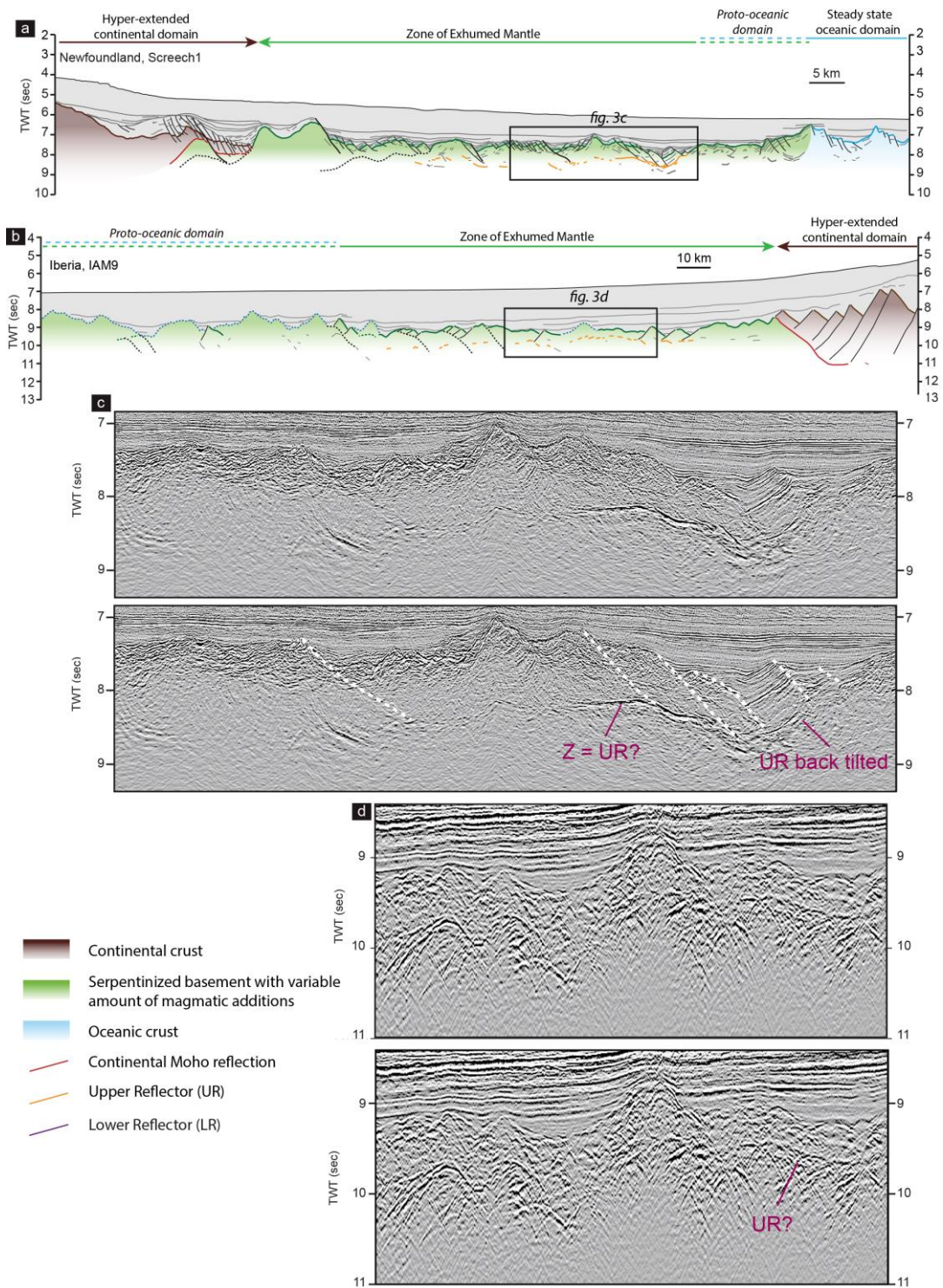
112 allochthons of continental origin) and the absence of clear and continuous Moho reflections (Minshull et
113 al., 1998; Gillard et al., 2015). These criteria can help to differentiate this domain from the adjacent
114 hyperextended continental and steady state oceanic crusts. Additional constraints may come from
115 refraction seismic data. P-wave velocities can range between 4.5 and 7 km/s for the upper 2 to 4 km of
116 basement, and an elevated velocity gradient of 1 s^{-1} is considered as characteristic for an exhumed mantle
117 domain (Chian et al., 1999). Based on gravity inversion results that use a mean crustal density of 2850
118 kg.m^{-3} , a basement composed of exhumed serpentinized mantle would appear as an approximately 3 km
119 thick crust (Cowie et al., 2015). This value contrasts with the thickness of standard magmatic oceanic crust
120 (e.g. Penrose crust) (~ 7 km; White et al., 1992; Bown and White, 1994) and the oceanward decreasing
121 thickness of hyperextended continental crust resulting in a wedge-shaped geometry (0 to 10 km, e.g.
122 Aslanian et al., 2009; Nirrengarten et al., 2016). While the transition from hyperextended continental crust
123 to exhumed mantle can be quite confidently distinguished, the transition to first steady state oceanic crust
124 is more controversial (Peron-Pinvidic et al., 2016; Peron-Pinvidic and Osmundsen, 2016). This zone of
125 uncertainty is currently referred to as “proto-oceanic domain” or “outer domain” (Gillard et al., 2015;
126 Peron-Pinvidic and Osmundsen, 2016; Sauter et al., 2018; Gillard et al., 2017; Tugend et al., 2018).

127 **2.1.Iberia-Newfoundland rifted margins**

128 The Iberia-Newfoundland conjugate rifted margins resulted from Late Jurassic-Early Cretaceous
129 rifting and opening of the southern North Atlantic (Tucholke et al. 2007; Nirrengarten et al., 2018). The
130 Iberia-Newfoundland conjugate margins are considered as the type example of a magma-poor rift system
131 because of the high density and diversity of the data sets acquired on these margins. In particular, the
132 distal domains are well described and the presence of a zone of exhumed continental mantle is attested
133 by several dredges (Boillot et al., 1980), ODP drill holes (Boillot et al., 1988; Sawyer et al., 1994; Whitmarsh
134 et al., 1998; Tucholke et al., 2004) reflection seismic surveys (Pickup et al., 1996) and refraction seismic
135 data (Dean et al., 2000; Funck et al., 2003; Whitmarsh et al., 1996).

136 Intra-basement reflections have been reported from the Screech 1 (Newfoundland margin) (Fig.3a)
137 and IAM9 (Iberian margin) (Fig.3b) reflection seismic lines (Hopper et al., 2004, 2006; Pickup et al., 1996;
138 Reston and McDermott, 2011) and occur in a domain where mantle is exhumed. On the Newfoundland
139 margin, a strong reflection is visible (“Z reflection”; Hopper et al., 2004, 2006) at approximately 1 sec TWTT
140 below top basement (Fig. 3c). To stay coherent with all the observations and to avoid confusion on the
141 nature of the reflectors, we will refer to the Z reflector as “UR” (Upper Reflector). The basement above
142 this reflector correlates with low P-wave velocities (4.3-4.5 km/s) (Funck et al., 2003). Note that the
143 resolution in that area is really low, meaning that these velocities are badly constrained and that there is
144 no mention about the velocity gradient in this layer. Immediately below the reflector, the underlying level
145 shows P-wave velocities of 7.6 km/s gradually increasing with depth to 8.0 km/s (Funck et al., 2003). At
146 the conjugate Iberia margin, a transparent upper basement layer is observed in the exhumed mantle
147 domain (Pickup et al., 1996) (Fig. 3d). The thickness of this layer varies between 0.5 and 1 sec TWTT. It
148 displays intermediate velocities (5.8-6.8 km/s) (Sibuet and Tucholke, 2012) and its base is marked by strong
149 reflectivity. Based on seismic refraction analysis, Minshull et al. (2014) showed that the first 3 km of
150 exhumed basement at the Iberia margin has a steeper velocity gradient (from 4.3 to 7.3 km/s) compared
151 to the deeper 3 to 6 km of basement (7.3 to 7.9 km/s).

152 A key observation is that normal faults can generally be interpreted as rooting into the UR (e.g.
153 Screech 1 line; Fig.3c). However, it can also be observed that the UR is sometimes back-tilted to the point
154 that it reaches the top basement. That suggests that the UR can also be affected by new exhumation faults
155 and potentially exhumed (Fig.3c).



156

157 Figure 3: Conjugate examples of non interpreted and interpreted seismic sections at (a) the Newfoundland distal margin

158 (Screech 1 line, interpretation from Gillard et al. 2016a) and (b) Iberian distal margin (IAM9 line). (c) and (d) Zooms of the

159 basement architecture in the zone of exhumed mantle at both margins, showing the presence of strong reflections (UR) at a
160 depth between 0.5 and 1 sec TWT below top-basement. The IAM9 seismic section is from Pickup et al. 1996.

161

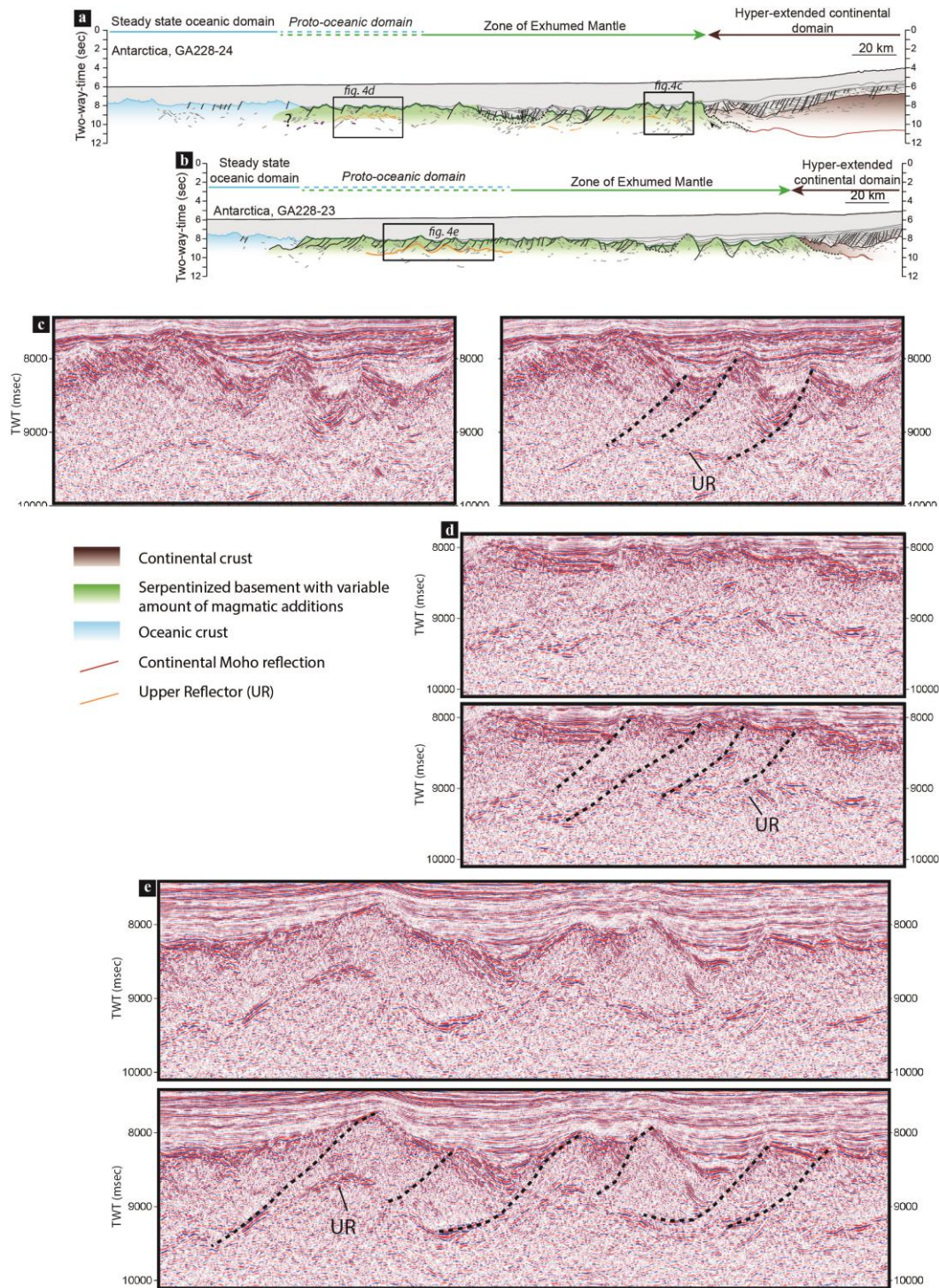
162 **2.2. East Antarctica rifted margin off Wilkes Land**

163 Rifting between Australia and Antarctica is postulated to have started during Callovian time (around
164 164 Ma; Totterdell et al., 2000) and rifting is recognized as polyphase (Ball et al., 2013; Gillard et al., 2015).
165 However, the age of final breakup and first oceanic crust is currently debated (Williams et al., 2019). The
166 presence of high-quality seismic reflection data enabled the architecture of the ultra-distal domains to be
167 interpreted as formed by a wide zone of exhumed mantle (Sayers et al., 2001; Direen et al., 2011; Ball et
168 al., 2013; Gillard et al., 2015). This interpretation is supported, at the western termination, by dredges of
169 serpentinized mantle rocks in the Diamantina Zone (Beslier et al., 2004).

170 Similar to the UR observed at the Iberia-Newfoundland margins, the Antarctic seismic sections from
171 AGSO survey GA228 (Stagg and Schiwy, 2002) show strong reflections localized at 1 sec TWTT below top-
172 basement (Fig. 4a, b). These reflections are often sub-horizontal (Fig. 4c, d). They are more or less
173 continuous throughout the exhumed mantle domain. In the Zone of Exhumed Mantle, the interpreted
174 normal faults generally root into the UR. However, in the most distal part (i.e., proto-oceanic domain of
175 Gillard et al., 2015) we observe a change in the morphology of this reflector. Indeed, UR is deformed, with
176 a similar morphology to top basement, which is marked by fault bounded, highly rotated blocks (Fig. 4e).
177 Further oceanward, an increase in extrusive magmatic additions is interpreted to seal normal faults that
178 formerly affected the exhumed basement (Gillard et al., 2016a) (Fig. 5a, c). In this domain, some normal
179 faults offset the UR and penetrate deeper into the basement (Fig. 5c, 6b).

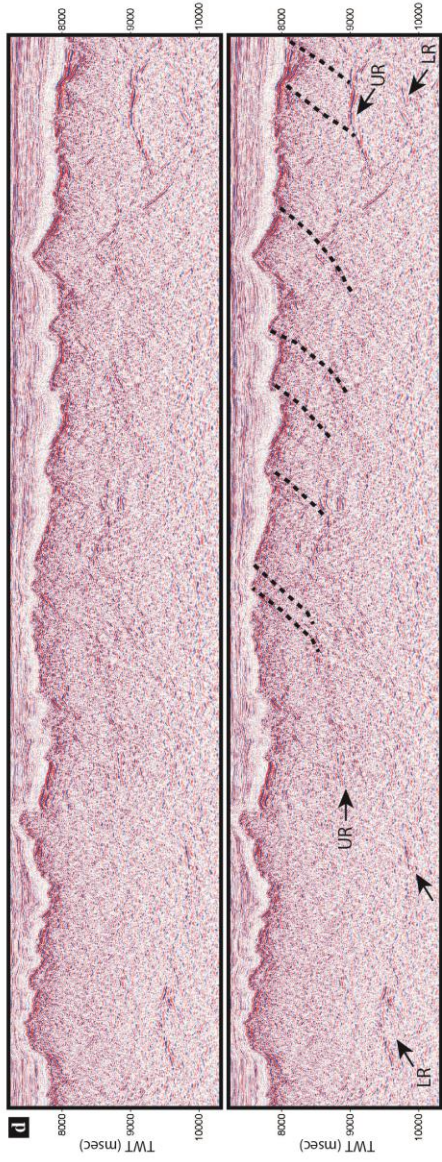
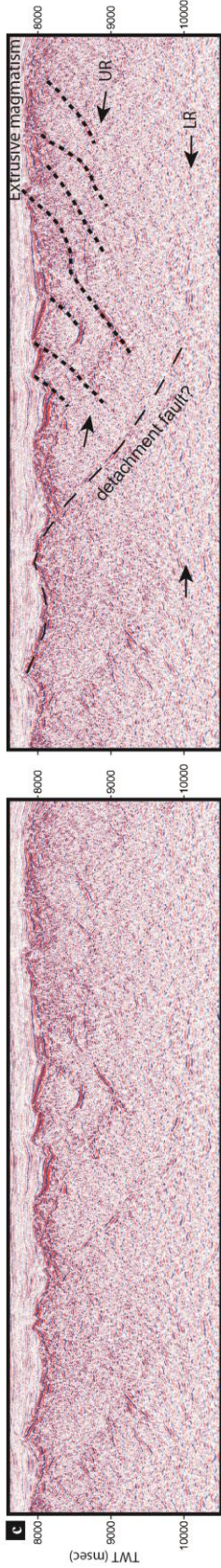
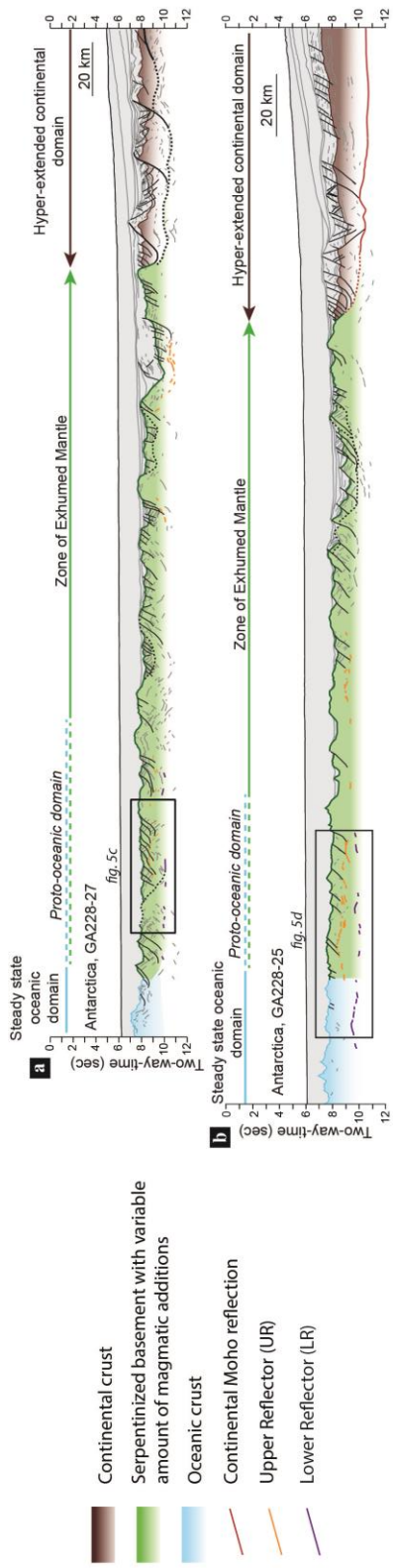
180 In addition to the UR, a second set of reflections is observed at this margin. These reflections,
181 hereafter referred to as the “LR” (Lower Reflectors), are generally observed between 1.5 and 2 sec TWTT

182 below the top basement (Fig. 5c, d, 6c). These deeper reflections are more subdued and sparsely visible
183 only in the interpreted proto-oceanic domain, close to the transition with the first steady state oceanic
184 crust. In contrast to the UR whose occurrence is always correlated with the presence of normal faults, only
185 few major faults also root on the LR (Fig.5c, 6c). Where it is the case, the UR is offset (Fig. 6e). It finally
186 appears that at some locations in the proto-oceanic domain, the UR and the LR can be observed together
187 (Fig. 5a, b; 6b).



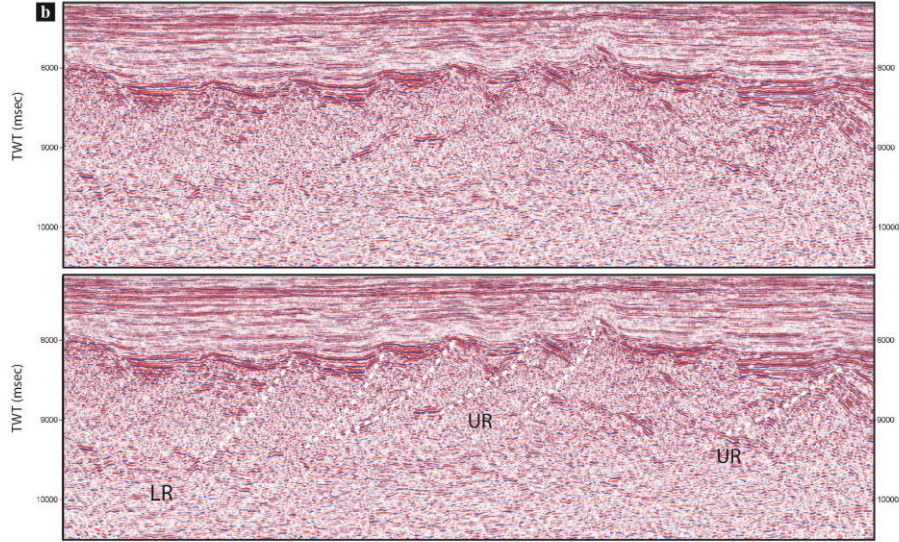
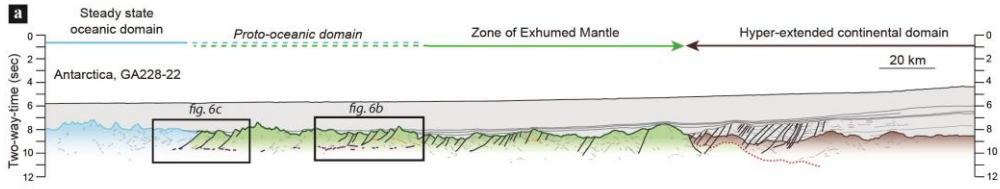
188

189 **Figure 4: Examples of non interpreted and interpreted seismic sections at the East Antarctica distal margin (interpretation from**
 190 **Gillard 2014). (a) Line GA228-24, (b) Line GA228-23. (c), (d), (e) show zooms displaying the architecture of the basement in the**
 191 **Zone of Exhumed mantle (c) and in the proto-oceanic domain (d) and (e) with the presence of UR. Copyright Commonwealth**
 192 **of Australia (Geoscience Australia)**

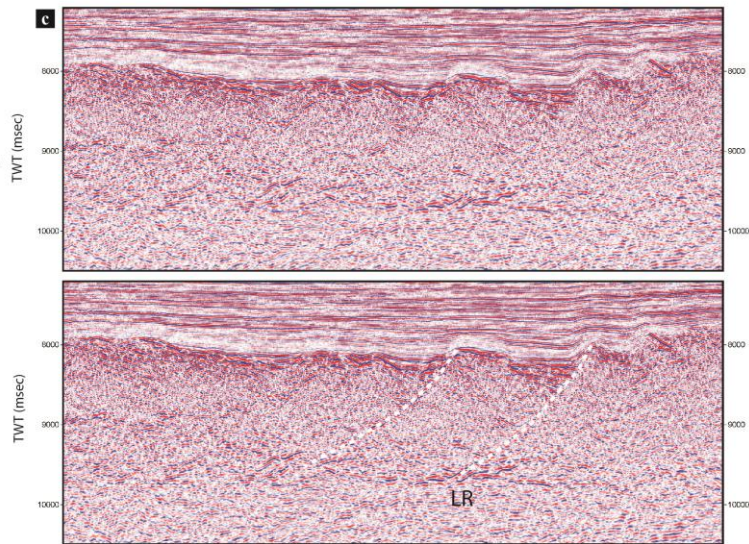


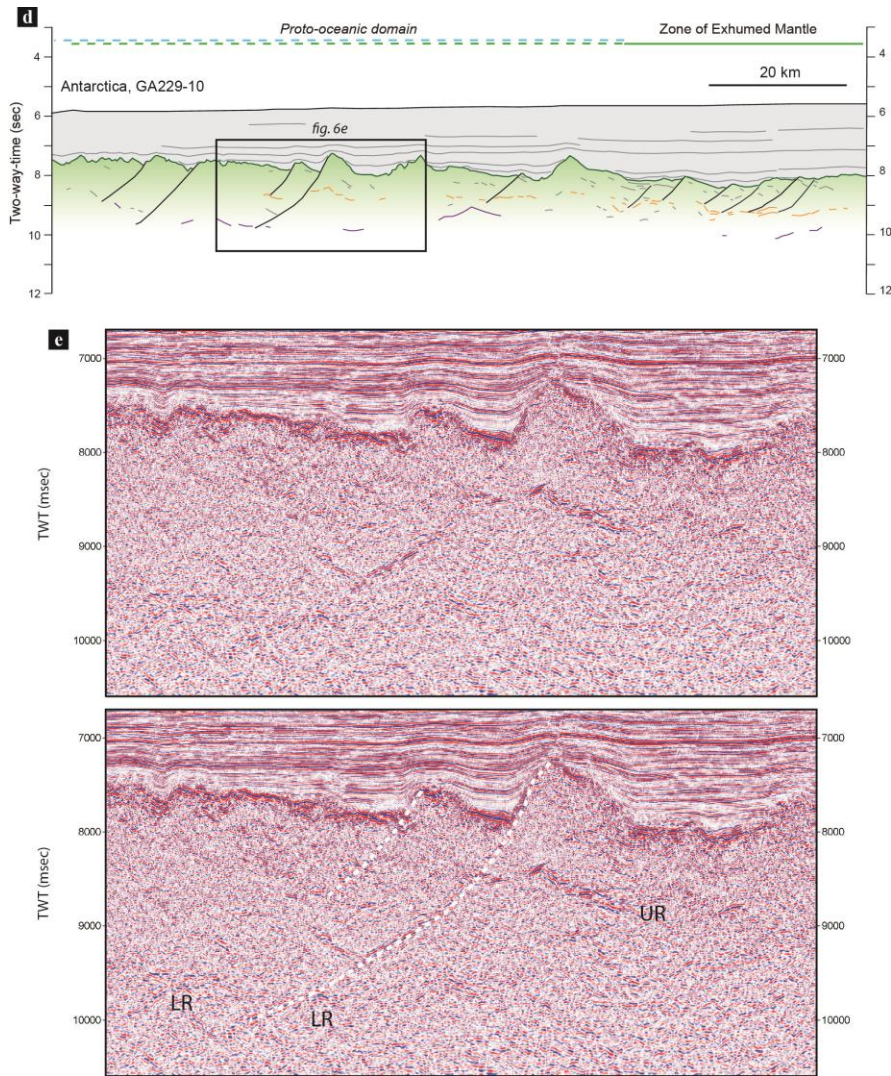
194 Figure 5: Examples of non interpreted and interpreted seismic sections at the East Antarctica distal margin (interpretation from
195 Gillard 2014). (a) Line GA228-27, (b) Line GA228-25. (c) and (d) show zooms of the basement architecture in the proto-oceanic
196 domain with the presence of UR and LR. *Copyright Commonwealth of Australia (Geoscience Australia).*

197



- Continental crust
- Serpentinized basement with variable amount of magmatic additions
- Oceanic crust
- Continental Moho reflection
- Upper Reflector (UR)
- Lower Reflector (LR)





199

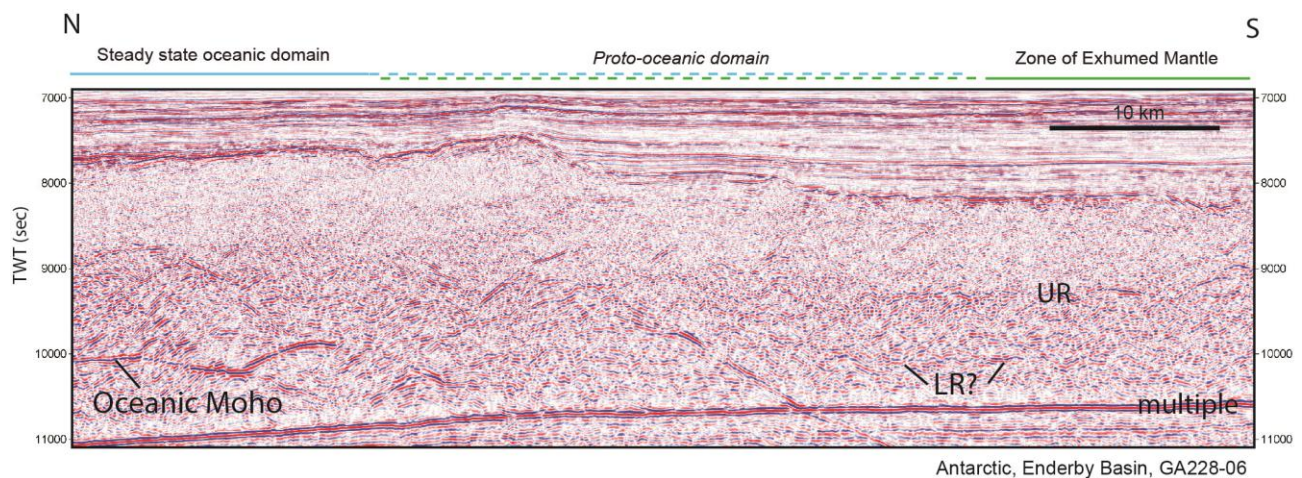
200 **Figure 6 : Examples of non interpreted and interpreted seismic sections at the East Antarctica distal margin (interpretation from**
 201 **Gillard 2014). (a) Line GA228-22, (b) and (c) show zooms of the basement architecture in the proto-oceanic domain with the**
 202 **presence of UR and LR. (d) Line GA229-10, (e) zoom of the basement architecture in the proto-oceanic domain with the presence**
 203 **of normal faults rooting onto a deep reflector (LR?), UR appears back tilted by the fault. Copyright Commonwealth of Australia**
 204 **(Geoscience Australia).**

205

206 **2.3. East Antarctica rifted margin off Enderby Land**

207 The margin off Enderby Land formed during the opening between East India and East Antarctica.
 208 Seafloor spreading in this area is thought to start in early Cretaceous (Gaina et al. 2007; Gibbons et al.

209 2013). Along this margin, the transition to steady state oceanic crust is clear and marked by a reflector
210 interpreted as the oceanic Moho (Fig. 7). This transition is also characterized by a step up of the top
211 basement and by a major change in the basement seismic character. The basement located south of this
212 transition is intensely faulted, with irregular intra-basement reflections and no visible seismic reflection
213 Moho. This basement has been referred to as a “transitional crust” (Stagg et al., 2004) and its nature has
214 not been determined. It is supposedly continental in origin (Stagg et al., 2004) and/or composed by
215 exhumed mantle (Gaina et al., 2007). The basement architecture is similar to that observed in the zone of
216 exhumed mantle in the previous examples (e.g. Fig. 6). It contrasts with the adjacent 2s TWTT thick oceanic
217 crust marked by a flat top basement and internal structure typical of magmatic oceanic crust (two sub-
218 horizontal layers: a transparent upper crust, and a highly reflective lower crust). We note an increase of
219 the extrusive magmatic supply near the step up marking the onset of oceanic crust. In particular, the
220 basement in the interpreted zone of exhumed mantle and proto-oceanic domain contains high amplitude,
221 horizontal reflections at 1s TWTT below the top basement, very similar to the UR previously observed.
222 Normal faults also root into that reflection (Fig. 7).



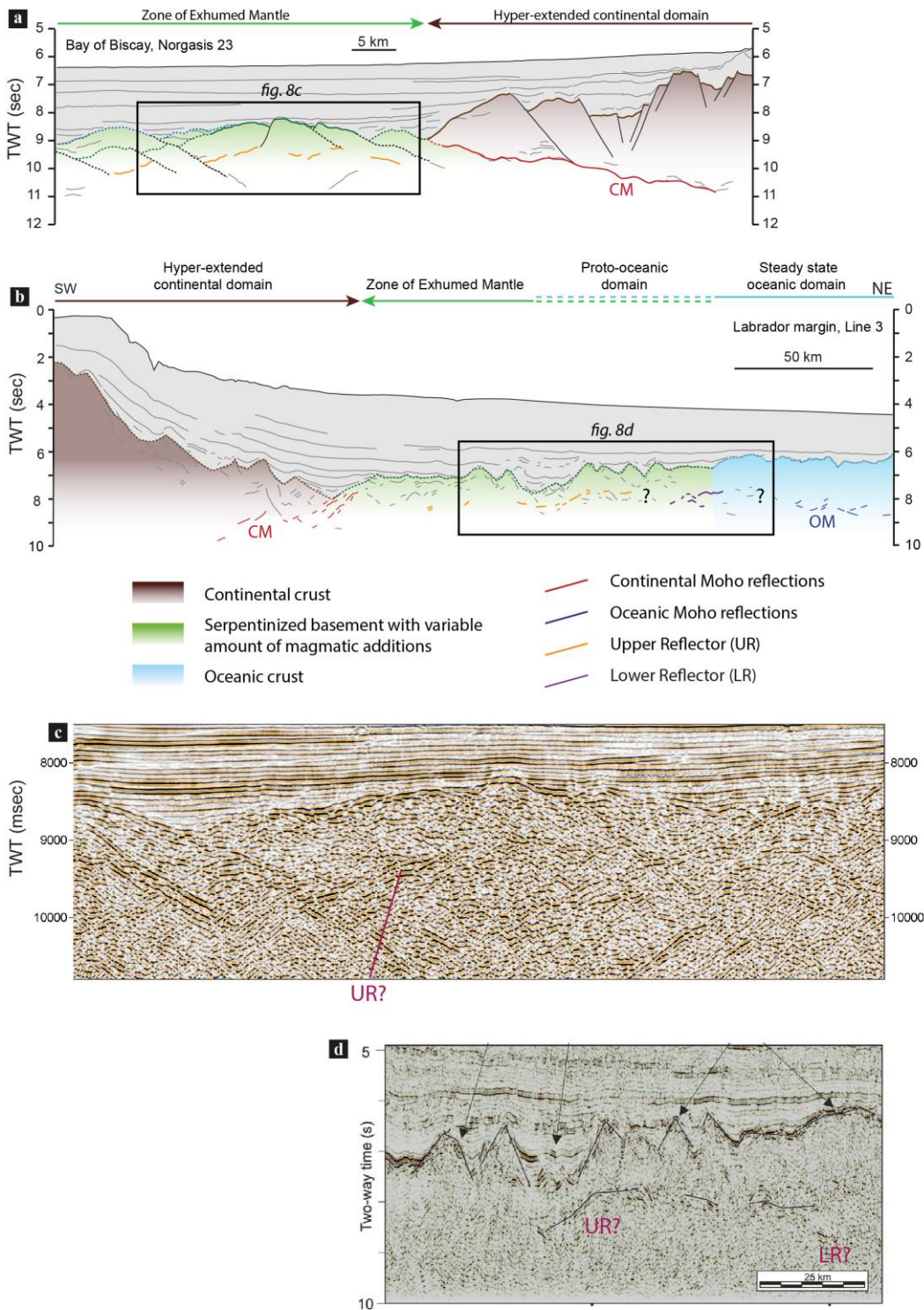
223
224 **Figure 7: Seismic profile along the Antarctica margin, in the Enderby Basin, showing the transition between the proto-oceanic**
225 **domain and the steady state oceanic domain. Copyright Commonwealth of Australia (Geoscience Australia).**

226

2.4. The Armorican rifted margin (northern Bay of Biscay)

227 The Bay of Biscay corresponds to a V-shape oceanic basin, bordered to the north by the Western
228 Approaches and Armorican margins. Following latest Jurassic to Early Cretaceous rifting, spreading
229 initiated in late Aptian to early Albian and stopped in the Campanian (e.g. Tugend et al., 2015; Montadert
230 et al., 1979). The first-order structure of the distal Armorican margin is constrained from both seismic
231 observations (Thinon et al., 2003) and gravity inversions (Tugend et al., 2014) indicating the potential
232 occurrence of a zone of exhumed serpentized mantle between hyperextended continental and oceanic
233 crusts.

234 Detailed seismic observations from the distal Armorican margin show different types of intra-
235 basement reflectors (Thinon et al., 2003). Here, we focus our observations along the exhumed mantle
236 domain of the NE-SW oriented Norgasis 23 seismic profile (Avedik and Olivet, 1994; Thinon et al., 2003)
237 (Fig. 8a and c). In this domain, the upper part of the basement is poorly reflective, being relatively
238 transparent and delimited at its base by discontinuous strong reflectors, located about ~1 s below the
239 interpreted top basement and roughly parallel to it (referred to “MS” in Thinon et al., 2003). The location
240 of this reflector in the exhumed mantle domain as well as its depth below top basement (about 1s) is
241 comparable to the UR described in the previous sections.



242
 243 **Figure 8: Interpreted seismic sections at (a) the Bay of Biscay (Norgasis 23 Line) and at (b) the Labrador margin (Line 3). CM:**
 244 **Continental Moho, OM: Oceanic Moho. The uninterpreted Norgasis 23 seismic section is available from Avedik and Olivet, 1994**
 245 **and was previously published in Thinon et al. 2003 and Labrador line 3 seismic section is from Keen et al. 2017. (c) Zoom of the**

246 basement architecture along the Norgasis 23 line showing the UR. (d) zoom modified from Keen et al. 2017 showing the
247 basement architecture and the presence of shallow reflections (comparable to UR).

248

249 **2.5. The Labrador rifted margin**

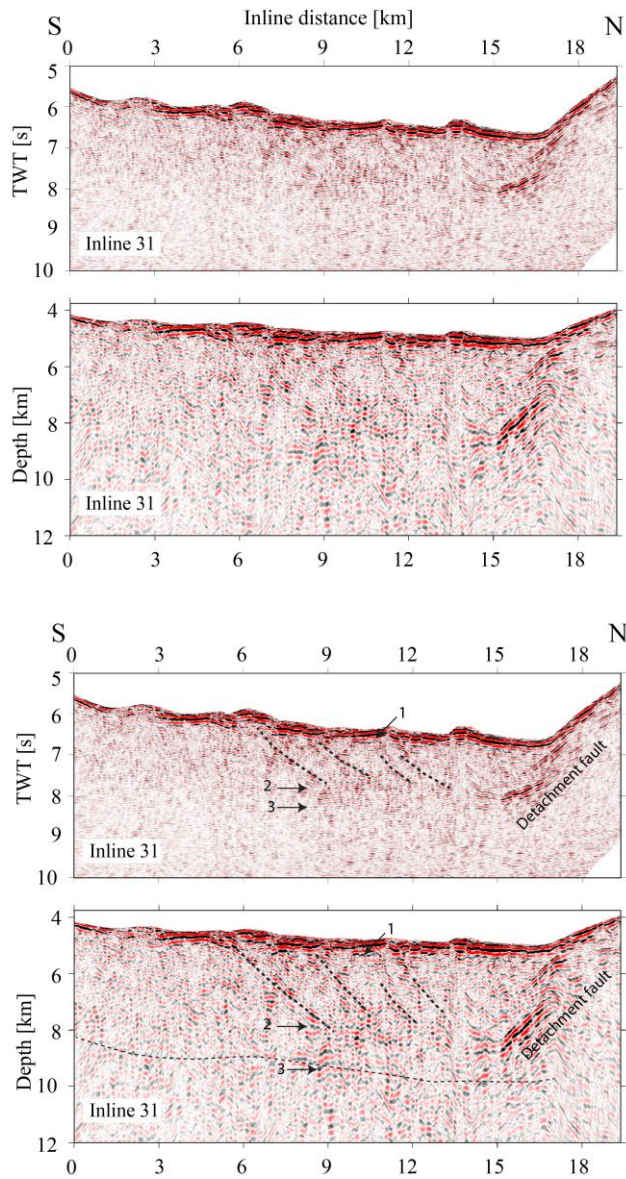
250 Rifting along the central Labrador margin initiated during the Early Cretaceous and breakup occurred
251 in Maastrichtian or Paleocene time (e.g., Oakey and Chalmers, 2012). Wide-angle reflection/refraction
252 data suggest the presence of a domain of exhumed serpentized mantle (Chian et al., 1995; Keen et al.,
253 1994, 2017). Discontinuous reflectors are visible below the top basement in the domains interpreted by
254 Keen et al. (2017) as the zone of exhumed mantle and the proto-oceanic domain (Fig. 8b). These reflectors
255 have been previously described by Chian et al. (1995) and referred to as “D” reflections. Even if the
256 reflectors are more discontinuous, it is here again possible to interpret two sets of reflections: UR and LR
257 (Fig. 8d).

258

259 **2.6. A present-day analogue: the axial valley of the Southwest Indian Ridge**

260 The easternmost part of the Southwest Indian Ridge (SWIR) is known to exhibit a smooth seafloor that
261 is almost entirely composed of seawater-altered mantle-derived rocks that were brought to the surface
262 by exhumation faults on both sides of the ridge axis over the last 10 Ma (Sauter et al. 2013). Recent seismic
263 acquisition in such an area of exhumed mantle shows the presence of several sets of intra-basement
264 reflections within the axial valley of the SWIR at 64°36'E (Momoh et al. 2017) (Fig.9): south-dipping, north-
265 dipping and sub-horizontal reflectors. The sub-horizontal reflectors occur just below the top basement (1
266 in Fig. 9), and between 1.5 sec TWTT (2 in Fig. 9) and 2 sec TWTT below top basement (3 in Fig. 9). While
267 the south-dipping reflectors have been interpreted as the active axial exhumation fault, the nature of the
268 other sets of reflectors is less constrained. Some of the north-dipping reflectors are not reaching top

269 basement and seem to be sealed by the shallowest group of sub-horizontal reflectors, which are
270 interpreted as magmatic sills (Momoh et al. 2017). These north-dipping reflectors also appear to root on
271 the top of the deepest group of sub-horizontal reflectors. These observations can be explained, similarly
272 to those reported from the Antarctica margin (see Fig. 5c), as normal faults affecting the oceanic exhumed
273 basement and rooting onto a decoupling level. The base of the deepest group of sub-horizontal reflectors
274 is located approximately at 2 sec TWTT below top basement and correlates with the 7.5 km/sec velocity
275 contour, which marks the transition from serpentinitized to fresh peridotites. The way these reflectors can
276 be compared to the UR and LR will be discussed later.



277

278 Figure 9: North-south time-migrated and depth-converted seismic sections imaging the axial valley of the Southwest Indian
 279 Ridge at 65°36'E (Momoh et al. 2017). In this area, dredge hauls that targeted the top basement recovered 97% serpentinized
 280 peridotites (Sauter et al. 2013). Small patches of lavas are erupted directly onto the detachment surface. Thin dashed black line
 281 represents the 7.5 km/s velocity contour (Momoh et al. 2017).

282

283 **3. Nature and origin of intra-mantle basement interfaces: constraints** 284 **from geological observations and quantitative analyses**

285 Our observations suggest that the UR and LR can be interpreted as distinct rooting levels for normal
286 faults, and thus correspond to different decoupling interfaces (décollement levels). However, their nature
287 and origin remain unclear from seismic observations only. Several hypotheses are possible to explain these
288 décollements, such as (1) detachment/exhumation fault planes, (2) shear zones, (3) brittle-ductile
289 transitions, (4) serpentinization fronts, (5) top of intrusive magmatic bodies (e.g., relict magma chambers).
290 All these décollement levels are potentially present in ultra-distal domains of magma-poor rifted margins.
291 As the mantle is likely exhumed and serpentinized in our case studies, we investigate the evolution of the
292 physical properties of serpentinized mantle rocks to interpret the potential nature of the UR and the LR.
293 Additional evidence of physical properties comes from outcrops that we consider as field analogues for
294 the LR.

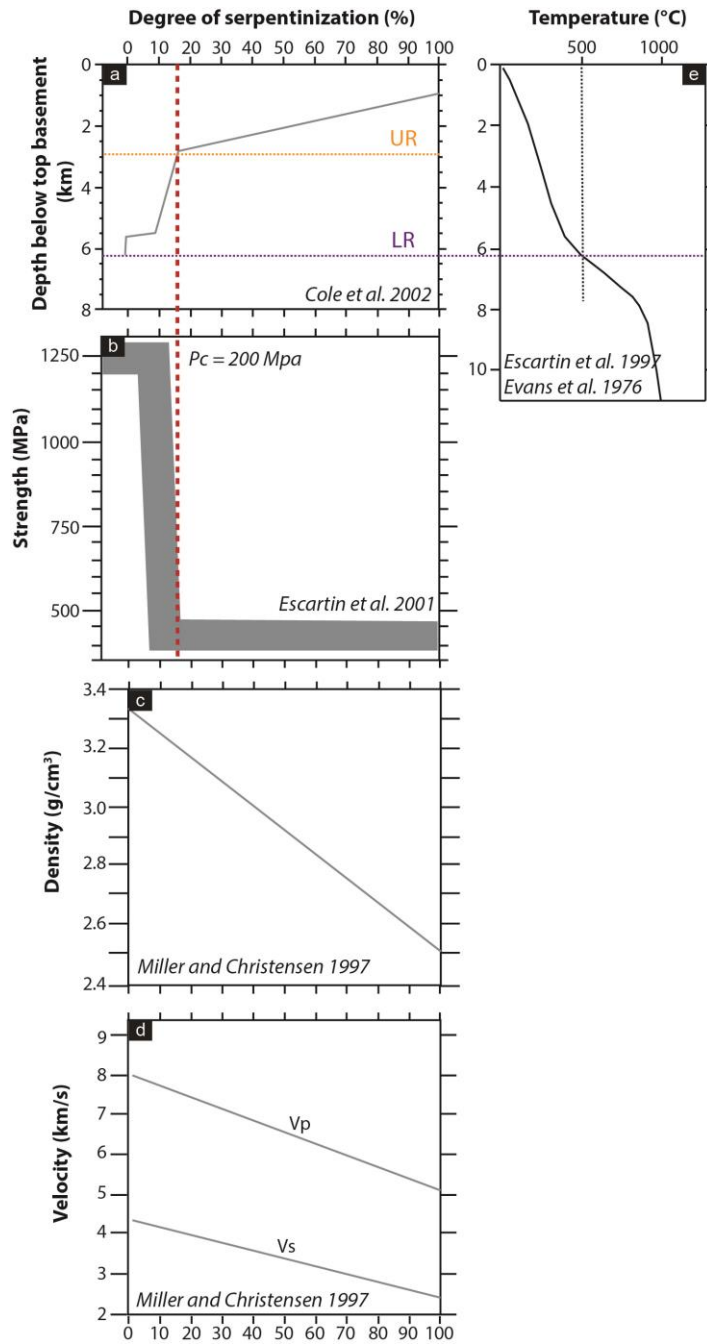
295 **3.1. Physical properties of serpentinized mantle rocks**

296 The hydration of mantle peridotites by seawater penetration along fault planes corresponds to the
297 serpentinization process, a reaction that occurs under a wide range of temperatures (from <100° up to
298 350°C) (Bonatti et al., 1984; Agrinier and Cannat, 1997; Mével, 2003; Decitre et al., 2002). During mantle
299 exhumation along a detachment fault the serpentinization process initially starts along the fault zone at
300 depths of 3 to 6km below top basement before propagating away from the fault plane, simultaneously
301 with volumetric expansion related to progressive unloading during footwall unroofing and rotation
302 (Andreani et al., 2007). When reaching the seafloor, mantle rocks are already strongly serpentinized. This
303 process leads to the formation of a basement with crustal p-wave velocities ranging between 4.5 and <8
304 km/s depending on the degree of serpentinization (Fig. 10). Strongly serpentinized peridotites at the top
305 basement progressively evolve into non-serpentinized peridotites at depth, as permeability reduces and

306 temperature increases. From a petrological point of view, there is no sharp boundary between
307 serpentinitized and non-serpentinitized mantle peridotites. In this sense, there is neither a Moho nor a crust-
308 mantle boundary in domains of exhumed mantle (Minshull et al., 1998). Serpentinization also reduces the
309 density compared to unaltered peridotite (from 3.3 to 2.5 g/cm³) (O'Hanley, 1996). It coincides with a
310 decrease of seismic velocities, from 8 to 7.5 km/s between 6 and 3 km below the top basement, and from
311 7.5 to 5 km/s from 3 km below top basement to the top basement (Miller and Christensen, 1997) (Fig.10).
312 These velocity ranges are comparable to what can be observed from refraction seismic studies for the
313 upper and lower basement layers at the Iberia-Newfoundland margins for example (Chian et al., 1999;
314 Dean et al., 2000).

315 However, despite the absence of a clear Moho discontinuity, intra-basement reflectors can still be
316 observed in the exhumed mantle and the outer/proto-oceanic domains of magma-poor rifted margins on
317 time migrated seismic sections, as shown previously (Fig. 3 to 8). Based on the refraction data of Minshull
318 et al. (2014) for the Iberia exhumed mantle domain, we can consider a velocity range of 4.3-7.3 km/s for
319 basement above UR (located at 1 sec TWT below top basement) and a velocity range of 7.3-7.9 km/s for
320 basement between UR and LR (located at 2 sec TWT below top basement). These velocities allow us to
321 calculate depth ranges for UR and LR: UR can be inferred to occur at 2.15 to 3.65 km below top basement
322 and LR at 5.8 to 7.6 km below top basement. It is interesting to note that the depth range of UR coincides
323 with abrupt changes in the mantle rock properties (Fig.10). Indeed, the evolution of the degree of
324 serpentinization is not linear; serpentinization quickly decreases from the top basement (about 100%) to
325 about 3 km depth, i.e. the depth-range of the UR, where it reaches ~15%. Below, it evolves more gently
326 before reaching the maximum depth of serpentinization (that is ~0%) at ~6.5 km, corresponding to the
327 depth-range of the LR (Fig.10). This maximum depth of serpentinization in exhumed mantle domains is
328 based on velocity measurements (e.g. Cole et al., 2002) and may coincide with the 450-500°C isotherm,
329 which represents the serpentine-olivine equilibrium temperature at ~0.2 GPa (Ulmer and Trommsdorff,

330 1999). Moreover, 15% serpentinization at a depth of approximately 3 km corresponds to a major change
331 in the mechanical behavior of hydrated peridotite (Fig.10). Indeed, the mechanical strength is very low
332 between complete and 15% serpentinization and rises abruptly for degrees < 15% approaching the
333 strength of unaltered dunite (Escartín et al., 2001). This abrupt change is related to the fact that serpentine
334 is mechanically much weaker than olivine and pyroxene, and has very low coefficients of friction (0.3
335 compared to 0.85 for unaltered peridotite) (Escartín et al., 2001). Brittle deformation in hydrated
336 peridotite is thus efficiently accommodated by shear cracks in the serpentinite (Escartín et al., 1997), even
337 for low degrees of serpentinization (Escartín et al., 2001). These results show that a major rheological
338 interface is expected to occur at a depth of approximately 3 km below top basement in exhumed mantle
339 domains.



340

341 Figure 10: Physical properties of serpentinized mantle rocks: (a) evolution of the degree of serpentinization with depth (from
 342 Cole et al. 2002), predicted from the velocity model of Dean et al. (2000) and following the relationship between velocity and
 343 serpentinization found by Miller and Christensen (1997) ; (b) evolution of the strength in function of the degree of
 344 serpentinization (from Escartin et al. 2001); (c) evolution of the density; and (d) velocity in function of the degree of
 345 serpentinization (from Miller and Christensen 1997); (e) evolution of the temperature with depth (from Escartin et al. 1997).

346 The abrupt change in the strength is highlighted in red and correlates with the depth of UR. The maximum depth of
347 serpentinization is highlighted in violet and correlates with the depth of the LR.

348 **3.2.Upper Reflector (UR): a major rheological interface**

349 The non-linear evolution of the degree of serpentinization with depth resulting in an abrupt
350 change in the mechanical behavior of hydrated peridotite at about 15% can explain the occurrence of a
351 décollement level at the depth where UR is observed (1 sec TWTT, Fig. 5). This décollement may represent
352 a major rheological interface created by the modification of the strain accommodation in the serpentinized
353 peridotite for serpentinization degree reaching approximately 15%. A seismic reflector (UR) at the depth
354 of this interface is likely the result of the combined effects of serpentinization and deformation. Normal
355 faults root into the previously created rheological interface and connect networks of serpentinized mantle.
356 This process enhances the formation of fault rocks (gouges) at the intersection between normal faults and
357 the rheological interface, in a similar way than proposed by Schuba et al. (2018) for the S-reflector at the
358 Galicia margin. Schuba et al. (2018) show that the reflection along the S-interface has been created by a
359 fault zone of 60 to 230m thick. In their attempt to model the seismic reflectivity along the Tasna
360 detachment fault, Hölker et al (2002) suppose a similar average thickness of 70m for the fault zone at the
361 top of the serpentinized peridotite and show that the seismic reflection can be caused by the slow-to-fast
362 velocity transition at the base of the damaged zone. That means that the reflectivity could not have been
363 created by the velocity contrast marking the transition between the continental crust and the
364 serpentinized peridotite damaged zone, but by intra-serpentinized peridotite velocity transition thanks to
365 the presence of the damage zone, which is more comparable to our case study. In our study, similar
366 thicknesses of the fault zone along the rheological interface could thus result in the observed seismic
367 reflections (UR). Moreover, the faults in the hanging wall will allow the water to easily penetrate at this
368 level, leading to hydration of the interface and resulting in additional serpentinization and strain
369 weakening. A similar process has been described by Bayrakci et al. (2016) along the hyper-extended

370 continental crust at the Galicia margin. It is likely that the presence of this hydrated interface controls the
371 deformation within the exhumed mantle. An alternative hypothesis is that the UR represents the
372 detachment fault plane buried under rider blocks (or extensional allochthons) in the rolling hinge model
373 (e.g. Buck 1988; Reston et al. 2007; Ranero and Reston 2011). The rolling hinge model would imply that
374 the UR is strictly of the same age than the normal faults rooting onto it. On the contrary, in the first
375 hypothesis the decoupling interface is created by a previous phase of mantle exhumation and can be
376 substantially older than the development of the normal faults. The observations that in the proto-oceanic
377 domain the UR is affected and cross-cut by normal faults (Fig. 4e, 5c, 6e) is for us inconsistent with the
378 rolling hinge model. Therefore, we favor the hypothesis that the UR is a rheological boundary related to
379 serpentinization processes.

380

381 **3.3. Lower Reflector (LR): a hydrothermal boundary or a major shear zone** 382 **in the mantle? Constraints from the Lanzo peridotite (Western Alps/N-** 383 **Italy)**

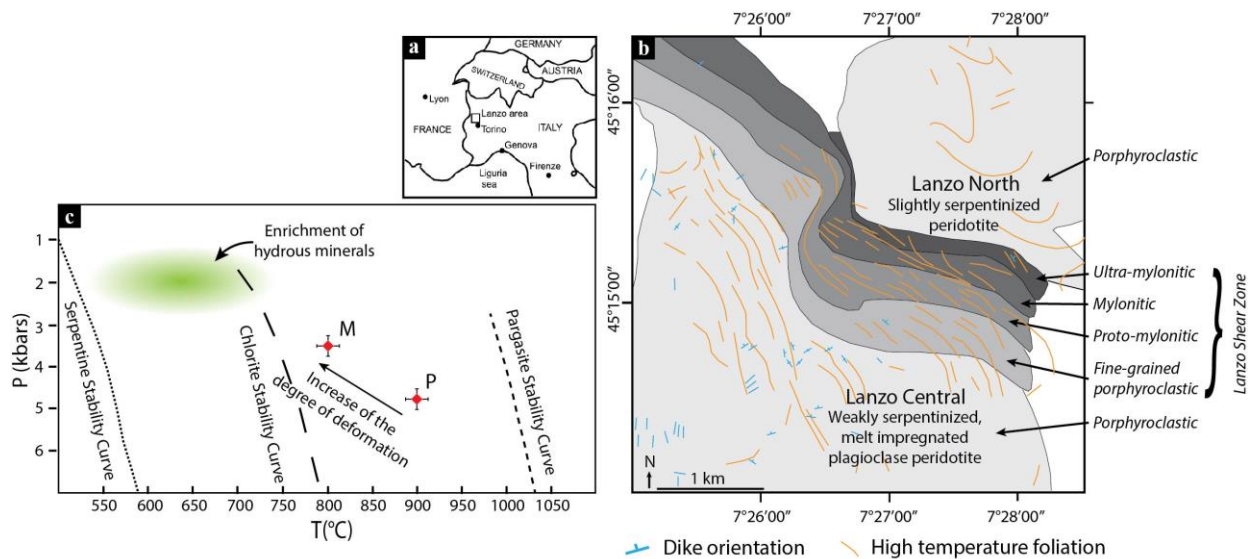
384 The LR, located at 2 sec TWTT (between 5.8 and 7.6 km) below top basement, appears to coincide with
385 the maximum depth of serpentinization, i.e. the “serpentinization front”. However, we do not expect to
386 observe this hydrothermal boundary on seismic sections since it does not coincide with an abrupt change
387 in the mineralogy of the mantle peridotite. Indeed, in contrast to the 15% interface, no clear rheological
388 discontinuity is expected to occur at the serpentinization front (Fig.10). In addition, the depth of the
389 serpentinization front is not necessarily stable (Cole et al., 2002), as it depends on a variety of parameters
390 such as permeability, thermal gradient and access to water. For example, upper mantle peridotites at
391 depth > 6 km below seafloor can be within the temperature range of serpentinization in the case of a
392 significant cooling effect caused by water circulation into the fault zones (Maffione et al., 2014). However,

393 on seismic sections, it can be observed that the rooting level of some faults corresponds with a reflector
394 (LR, Fig. 5, 6), suggesting the presence of a decollement level at 2s TWTT. If the serpentinization process
395 cannot account for this observation, other processes, such as magmatism and/or shear zones may explain
396 the LR. This reflector is too deep to be directly drilled at present day rifted margins. The only way to
397 investigate further the nature of the LR is to study fossil analogues.

398 Here we consider the Lanzo shear zone as a potential analogue of the LR observed on seismic
399 sections from magma-poor rifted margins. The Lanzo shear zone is exposed in the Lanzo massif in
400 northwestern Italy, north of Torino (Fig. 11a). The Lanzo massif is composed of weakly to fully
401 serpentinized peridotites, exhumed during the opening of the Jurassic Alpine Tethys ocean (Müntener and
402 Piccardo, 2003; Kaczmarek and Müntener, 2008; Nicolas et al., 1972; Kaczmarek and Müntener, 2010).
403 The Lanzo shear zone corresponds to a kilometer-scale, mylonitic shear zone juxtaposing weakly
404 serpentinized, melt impregnated plagioclase peridotites (Lanzo Central) (Kaczmarek and Müntener, 2008;
405 Nicolas et al., 1972; Bodinier, 1988) against more serpentinized mantle rocks (Lanzo North) (Fig. 11b).
406 Similar shear zones in mantle peridotites have also been observed in the Ligurian ophiolites (Northern
407 Apennines, Italy; Tribuzio et al., 1995), in the Erro Tobbio peridotites (Hoogerduijn Strating et al. 1991) or
408 in the Platta unit (Müntener et al. 2010). Microstructural evidence indicates that these shear zones were
409 active at high temperature (700 to 900°C), with low or no involvement of seawater-derived fluids (Tribuzio
410 et al., 1995; Sanfilippo and Tribuzio, 2011). The ductile deformation occurred therefore deeper in the
411 mantle, below the serpentinization front, associated with mantle exhumation and/or magma-
412 emplacement. Indeed, the formation and evolution of the Lanzo shear zone appears strongly related to
413 melt-rock reactions coupled with active deformation (Müntener and Piccardo, 2003; Kaczmarek and
414 Müntener, 2008, 2010; Higgie and Tommasi, 2014). Progressive deformation is witnessed by the
415 development of textures evolving from porphyroclastic to fine-grained porphyroclastic, to proto-mylonitic,
416 to ultramylonitic (Kaczmarek and Müntener, 2008; Kaczmarek and Tommasi, 2011). Mineral chemistry,

417 microstructures and thermometry of the Lanzo shear zone suggest that strain localization began at
418 temperature > 1000°C in the lithospheric mantle (Kaczmarek and Müntener, 2008), i.e. at depth of
419 approximately 12-15 km (pressure of 4.4 kbar, Fumagalli et al., 2017) (Fig. 11c). In particular, it appears
420 that melt rock reaction in the subcontinental mantle started before the onset of the high-temperature
421 shearing, favoring localization of deformation (Holtzman et al., 2003; Kohlstedt and Holtzman, 2009;
422 Holtzman and Kendall, 2010). The degree of deformation and strain localization along the Lanzo shear
423 zone progressively increases together with the decrease of the pressure and temperature and with grain
424 size reduction (Kaczmarek and Müntener, 2008; Fumagalli et al., 2017; Linckens et al., 2011) (Fig. 11c). This
425 suggests a progressive uplift of the shear zone at shallower lithospheric levels. The actively deforming
426 shear zone appears to focus migrating liquids and then to act as a permeability barrier due to grain size
427 reduction. The plagioclase peridotite mylonites observed along the Lanzo shear zone formed at ~3 kbars,
428 thus approximately at 9 km depth (Fumagalli et al., 2017) and below ~850°C (Kaczmarek and Müntener,
429 2008). It is interesting to note that the dynamically recrystallised ultra-mylonites locally contain retrograde
430 Cl-rich hydrous minerals (amphibole and chlorite, Vieira Duarte, *personal communication*) that formed at
431 temperatures higher than the serpentine stability (Kaczmarek and Müntener, 2008), suggesting that the
432 shear zone finally reached the base of the hydrothermal front, i.e. about 6 to 7km as is the case for the LR.
433 This suggests that during the latest stage of the margin evolution, the mylonitic shear zone can also
434 coincide with the rooting level of late exhumation faults, which can locally penetrate and exhume the
435 shear zone to the seafloor. An example of an exhumed mylonitic shear zone is observed at the Chenaillet
436 Ophiolite (Manatschal et al., 2011), where Jurassic gabbros show a high temperature mylonitic shear zone
437 truncated by low temperature, hydrated fault zones corresponding to extensional detachment faults. The
438 mylonites and ultramylonites observed in the gabbros formed at temperatures between 700°C to 800°C
439 (Mevel et al., 1978), i.e. at similar conditions like those observed along the Lanzo shear zone. Moreover,
440 the Chenaillet mylonites show evidence for syn-tectonic magmatism that have been affected by fluids after

441 exhumation of the rocks along the shear zone (Mevel et al., 1978; Manatschal et al., 2011). The scale of
 442 the Lanzo shear zone, which is about 1 km wide, makes this structure an interesting case for its
 443 interpretation as an analogue of the LR. The presence of a sub-horizontal mylonitic shear zone in the
 444 peridotite flooring the serpentinization front could indeed explain the origin of the LR in the proto-oceanic
 445 domain. Moreover, the melts percolating at the level of the shear zone will also likely create the impedance
 446 contrast necessary to obtain seismic reflections at this level. The Lanzo shear zone provides an explanation
 447 for large-scale decoupling horizons between the serpentinized and non-serpentinized, plagioclase-bearing
 448 mantle peridotites.



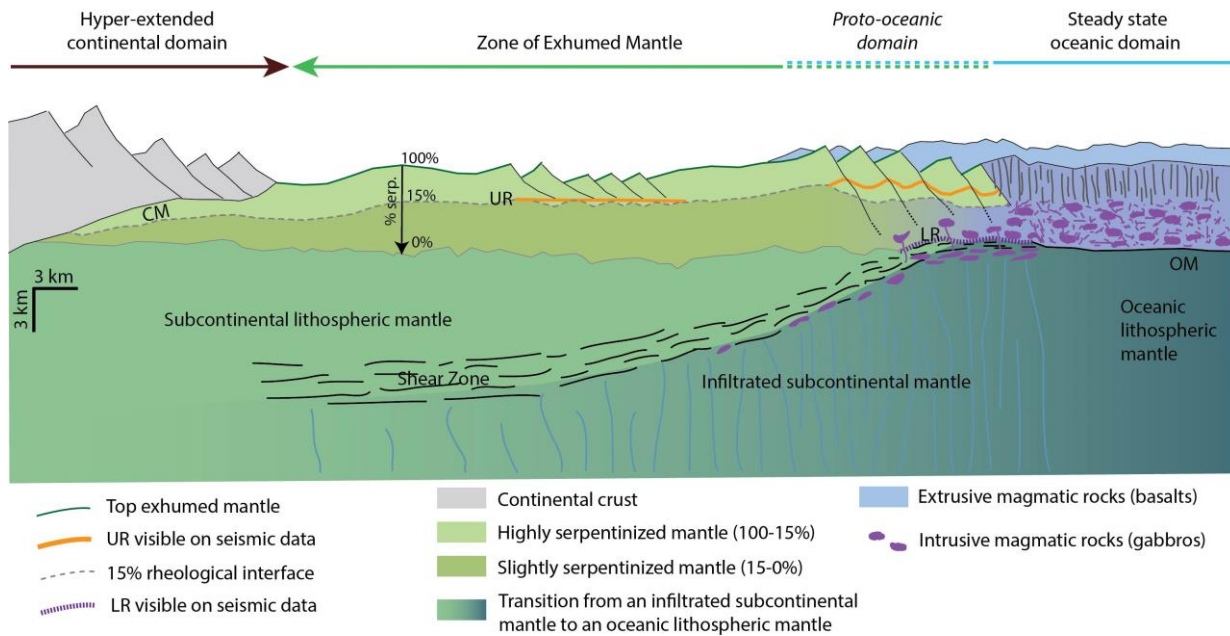
449
 450 **Figure 11: (a) Location of the Lanzo massif. (b) Map of the Lanzo Shear Zone modified from Kaczmarek and Müntener, 2008. (c)**
 451 **Simplified Pressure-Temperature diagram illustrating the evolution of the deformation for the Lanzo Shear Zone and the**
 452 **beginnings of hydration above serpentine stability (P: porphyroclastic textures; M: mylonitic textures; Pargasite stability after**
 453 **Niida and Green, 1999; Chlorite and serpentine stability after Ulmer and Trommsdorff, 1999). Pressure-temperature estimates**
 454 **and errors (± 0.5 kbars and $\pm 25^\circ\text{C}$) of the plagioclase peridotite are from the FACE barometer (Fumagalli et al., 2017).**

455 **4. Discussion**

456 **4.1. Serpentinization and accommodation of extensional deformation**

457 Seismic and field studies show the presence of two major distinct decoupling levels in the basement
458 of ultra-distal domains at magma-poor rifted margins. These decoupling levels are at different depths and
459 appear to be associated with different processes. In the upper part of the lithosphere, extension is
460 manifested by mantle exhumation along detachment faults. The serpentinization process occurring along
461 these active exhumation faults leads to the formation of a major rheological interface at approximately 3
462 km below seafloor. This efficient decollement level is highlighted by the presence of numerous normal
463 faults rooting into this interface (UR, Fig. 4). This rheological interface thus appears to be a key factor for
464 the organization of the deformation during the mantle exhumation stage. Indeed, it allows mechanical
465 decoupling between the shallowest, brittle/frictional part of the lithosphere, and deeper levels that
466 accommodate the deformation along mylonitic shear zones.

467 In our hypothesis the decoupling surface at 3 km below seafloor will allow for a constant re-
468 organization of the deformation due to exhumation and serpentinization in the upper part of the
469 continental lithosphere (Gillard et al., 2015, 2016b, 2016a). This is associated with magma emplacement
470 and thermal perturbations in the lower part of the continental lithosphere (Fig. 12). The complex
471 interaction between the upper and lower parts of the continental lithosphere, and the successive rising of
472 the asthenosphere may explain the transition from asymmetric structures during early exhumation to
473 finally symmetric structures during lithospheric breakup (Gillard et al., 2016b).



474

475 **Figure 12: Snapshot summarizing at a final stage the main observations and the processes leading to the formation of the**
 476 **interfaces UR and LR. CM: Continental Moho; OM: Oceanic Moho.**

477 The thinning of the continental lithosphere, associated with mantle exhumation, will passively uplift
 478 the deep shear zone, from depth of 12-15 km to the base of the hydrothermal front (6-10 km) (Kaczmarek
 479 and Müntener, 2008) (Fig.12). Indeed, contrary to previous studies proposing that exhumation faults were
 480 lithospheric-scale structures rooting at the lithosphere-asthenosphere boundary (Lemoine et al., 1987;
 481 Boillot and Froitzheim, 2001; Wernicke, 1981), several observations from oceanic core complexes and
 482 fossil rifted margins argue for a shallower rooting depth (6-10 km), at or just below the hydrothermal front
 483 (deMartin et al., 2007; Manatschal et al., 2011).

484 Our observations from seismic reflection and field studies suggest that during the first stage of
 485 mantle exhumation, faults are rooting on decoupling levels controlled by the degree of serpentinization.
 486 The accommodation is thus mainly tectonic and controlled by hydration reactions (Fig. 12, 13). However,
 487 during the development of the proto-oceanic domain, the UR is deformed by faults that seem to root at
 488 deeper levels (Fig. 6, 12). This evolution is associated with an increase of the magmatism extruded on top

489 of the basement (Fig. 5a, c) and with the progressive appearance of the LR. These observations suggest
490 that magmatism could play a key role in developing the new interface controlling the rheology of extending
491 mantle during the formation of the proto-oceanic domain and final breakup.

492

493 **4.2. Distribution of magmatic rocks and influence on the structural** 494 **evolution**

495 The proto-oceanic domain show increasing evidence for of magmatic rocks at the top basement
496 and is marked by the appearance of a deep reflector (LR) on seismic sections (Fig. 6). However, the
497 presence of magmatic material at the top basement also suggests that part of magmatic material must
498 also be stored at depth. Indeed, the emplacement level of magmatic rocks is partly controlled by buoyancy
499 forces; magma might stagnate at levels of neutral buoyancy until they have fractionated and reacted to
500 the point where magma density is less than that of the surrounding host rock (Ryan, 1993). Another
501 possibility is that magma migration terminates when reaching an actively deforming “freezing horizon”
502 (Morgan and Chen, 1993; Kohlstedt and Holtzman, 2009; Sparks and Parmentier, 1994). In this case, there
503 could be a link between magma emplacement and strain localization. This last interpretation would be
504 coherent with the observations made at the Lanzo Shear Zone (Kaczmarek and Müntener, 2008). Indeed,
505 Kaczmarek and Müntener (2008) and Higgle and Tommasi (2014) showed that small gabbro dikes and sills
506 are mainly distributed below, and sometimes parallel to the mylonitic shear zone in the Lanzo peridotite
507 (Fig. 11). The reduction of permeability associated with the formation of the mylonite, perhaps coupled to
508 the cooling effects of the hydrothermal front, could form a thermal boundary controlling the upward
509 migration and crystallization of mafic melts in the proto-oceanic domain. The net result is the
510 emplacement of gabbro sills during shearing (Kaczmarek and Müntener, 2008) at or just below the
511 hydrothermal front, i.e. close to the depth of the LR. In addition to the fact that the LR could represent a

512 shear zone, the presence of intrusive magmatic material along this horizon could also explain its
513 reflectivity. The sub-horizontal reflectors observed between 1 and 2 sec TWTT below top basement in the
514 axial valley of the SWIR (Fig. 9) have been interpreted as magmatic intrusions above the transition from
515 fresh to serpentinized peridotites (Momoh et al. 2017). However, the observation that normal faults are
516 rooting onto these reflectors (Fig. 9) indicates some analogy with the UR reflections observed at the
517 different studied magma-poor rifted margins. Indeed, the thermal, magmatic and hydration conditions
518 occurring at the SWIR are comparable to the ones that occurred during the evolution of the exhumed
519 mantle domain at magma-poor rifted margins, leading to the development of similar serpentine-related
520 structures such as the UR. In contrast, it is not clear if the deepest reflectors in the oceanic basement at
521 the SWIR can be compared to the LR observed at magma-poor rifted margins. Indeed, the very low
522 magmatic budget recognized at the SWIR (Sauter et al. 2013) is likely different to the one involved during
523 the development of the proto-oceanic domain, where the LR occurred. This latest domain should rather
524 be compared with Oceanic Core Complexes, which are recognized as more magmatic systems than the
525 exhumed mantle domains of the SWIR (Tucholke et al. 2008). In addition, strong subhorizontal reflectors
526 have been observed in reflection images at the Rainbow Core Complex (Mid-Atlantic Ridge), at
527 approximately 6 km below top basement, where mantle derived rocks have been dredged (Dunn et al.
528 2017; Canales et al. 2017). These reflectors have been interpreted as cooling melt bodies intruded into the
529 massif, their heat driving the fluid circulation (Dunn et al., 2017). It would be interesting to deeply
530 investigate the comparison between the LR and intrusive magmatic bodies at Oceanic Core Complexes.
531 However, it is possible that the LR is a structure specific to magma-poor rifted margins, as we propose that
532 it is linked both to the increasing magmatic budget and to a shear zone associated to the processes of
533 continental lithospheric extension.

534 Similar to what has been proposed for the Rainbow Core Complex (Dunn et al. 2017), we propose
535 that the presence of partially molten intrusions close to the hydrothermal front will change the thermal

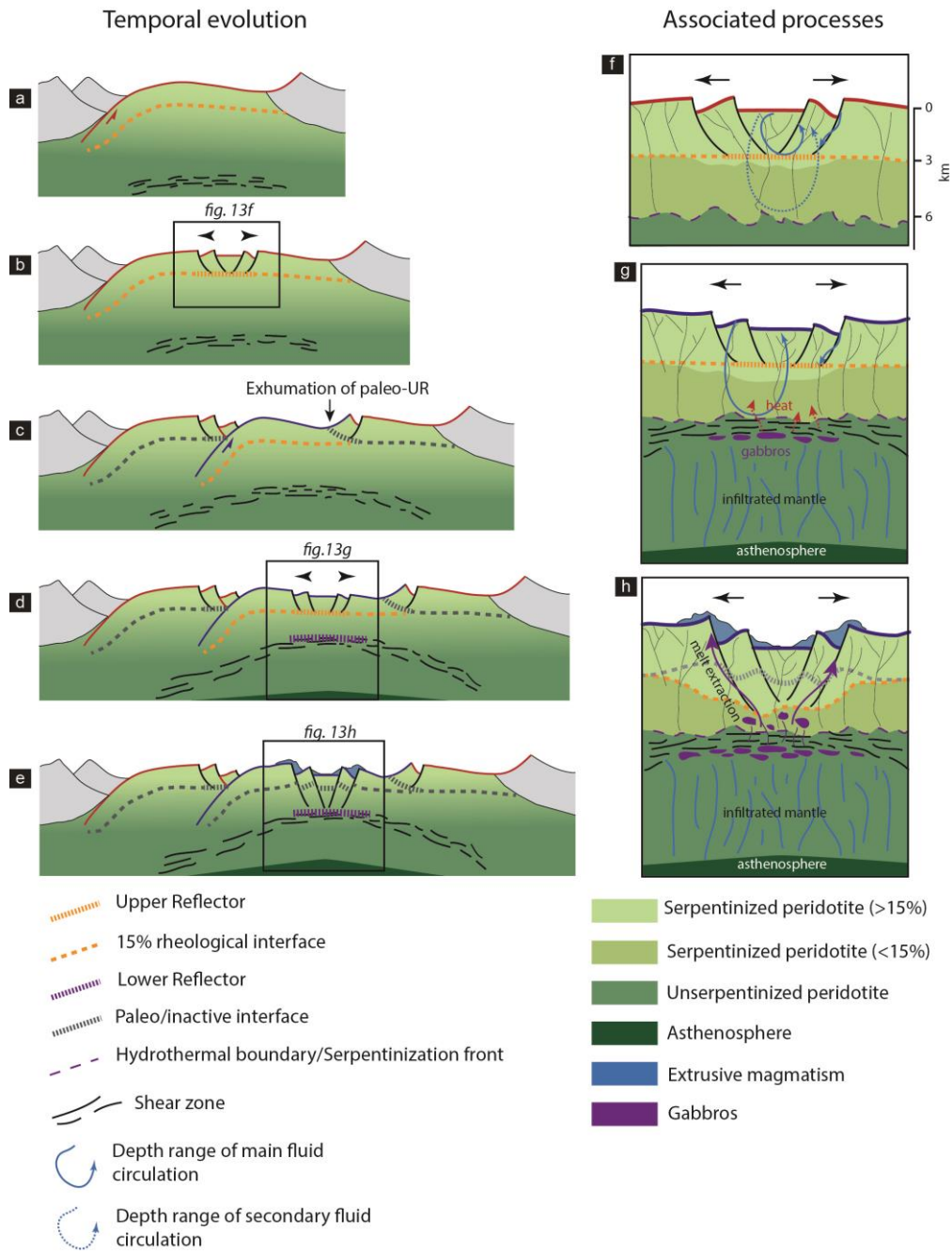
536 and hydration conditions in the proto-oceanic domain of the studied magma-poor margins. As a
537 consequence, the rheological structure of the basement is transient, and normal faults are able to
538 penetrate deeper than the UR and possibly connect to the LR (Fig. 6, 12). Moreover, it has been observed
539 on seismic sections that extrusive magmatism in the proto-oceanic domain is often present at the
540 breakaway of these normal faults (Fig. 6). This is similar to what has been mapped in field analogues
541 (Chenaillet Ophiolite), where it has been suggested that normal faults act as feeder systems for extrusive
542 magmatism (Manatschal et al., 2011). We propose that in this domain, normal faults are able to penetrate
543 sufficiently deep to extract melt stored along the LR interface.

544

545 **4.3. Synthesis of the structural and magmatic evolution**

546

547 We summarize here the key steps in the structural and magmatic evolution of the distal domain
548 at magma-poor rifted margins in the conceptual model shown in Fig. 13.



549

550 **Figure 13: Geologic model showing the temporal evolution of the distal margin with specific focus on the formation and**
 551 **evolution of the different decoupling interfaces in distal domains of magma-poor rifted margins. Zooms highlighting the**
 552 **processes (hydration, shearing, magmatism) and their interactions associated to the formation/evolution of the decoupling**
 553 **interfaces.**

554 Following the hyperextension stage, the separation of the continental crust occurs in a magma-poor
555 context, leading to an accommodation of the extension by mantle exhumation along detachment faults
556 (Fig. 13a). At depth, the thinning of the lithosphere is accommodated by the formation of a wide shear
557 zone. The strain localization at depth is favored by melt-rock reactions. The hydration process associated
558 with detachment faulting leads to the formation of a strong rheological interface at the level of 15% of
559 serpentinite, which is approximately located at a depth of 3 km below seafloor (Fig. 13a). The exhumation
560 fault becomes progressively inactive and extensional deformation tends to migrate in the area where the
561 asthenosphere is rising (Fig. 13b). This re-organization of the deformation is controlled by the activation
562 of the rheological interface that is used as a decoupling level for normal faults (visible as UR on seismic
563 sections) (Fig. 13f). The fluid circulation along active normal faults can lead to a new generation of
564 serpentinization just below the pre-existing UR interface, probably preconditioning the initiation of a new
565 exhumation fault (Fig. 13c). At this stage, the UR can be exhumed at the top-basement as a paleo-
566 decoupling interface (Fig.3; 13c). As extension and mantle exhumation continues, extensional deformation
567 along the deep shear zone will localize and evolve towards the formation of peridotite mylonites as the
568 shear zone is progressively exhumed at shallower depths and lower temperatures. As the subcontinental
569 lithosphere thins, melt infiltration in the mantle below the shear zone will increase (Picazo et al., 2016),
570 but the reduction of the permeability in the shear zone will act as a barrier for the upward melt migration.
571 The shear zone will finally reach the base of the hydrothermal front, which can be approximately at 6-7
572 km (Fig.13d). At this stage, the presence of plagioclase peridotite and/or partially crystallized gabbroic
573 bodies just below the hydrothermal front will impact the rheology of the upper serpentinized layer (Fig.
574 13g). Normal faults are thus able to penetrate deeper and to extract some of the melt, which was stored
575 at depth (Fig. 13e, h). In reaching the hydrothermal front, the shear zone also reaches the depth where it
576 can be sampled by potential new exhumation faults. It is thus possible to exhume infiltrated mantle at the
577 seafloor, represented by plagioclase peridotite, re-fertilized by melt percolation, as observed for example

578 in the Platta nappe or Chenaillet Ophiolites (Muntener et al., 2004; Picazo et al., 2016; Muntener et al.,
579 2010). This final stage could thus be referred to as the lithospheric breakup (Tugend et al., 2018; Peron-
580 Pinvidic and Osmundsen, 2016), marking the end of rifting and recording the onset of seafloor spreading.

581

582 **5. Conclusions**

583 Based on seismic observations, we highlighted the presence of two main intra-basement decoupling
584 interfaces in the exhumed mantle domain at magma-poor rifted margins. Integrating physical properties
585 of serpentinized rocks and constraints from Alpine field analogues allowed us to interpret and discuss the
586 nature and origin of these interfaces. In particular, our results show the presence of a strong rheological
587 interface at about 3 km below top basement. We suggest that this interface played a major role in the
588 organization of the deformation during the evolution of the exhumed mantle domain. The presence of a
589 second, deeper interface occurring in the proto-oceanic domain seems to be the result of interactions
590 between tectonic, hydrothermal and magmatic processes, which will modify the rheology of the
591 serpentinized basement in this domain. It is interesting to note that during the formation of the proto-
592 oceanic stage, the deformation of the upper and lower layers is progressively coupling, contrary to
593 previous stages where the upper deformation was not directly linked to the deformation at depth. This
594 change could be a signature of the proto-oceanic domain, together with the increase of magma
595 emplacement at the seafloor. Indeed, this final coupling of the deformation, associated with the breakup
596 of the continental lithosphere, marks the localization of the deformation and the initiation of a stable
597 spreading center.

598

599 **Acknowledgement**

600 Seismic lines of the Antarctic surveys GA228 and GA229 were provided by Geoscience Australia after
601 personal request and are published with the permission of Geoscience Australia. We also would like to
602 thank I. Thinon and Ifremer for providing us the Norgasis 23 reflection seismic profile presented in this
603 work. We kindly acknowledge Ekeabino Momoh for discussion and for the seismic image of the SWIR. This
604 research was supported by Exxon Mobil as part of the CEIBA II project. We greatly thank Christopher A.
605 Johnson and Anne-Marie Karpoff for useful and often in-depth discussions, as well as constructive
606 comments by Tim Minshull and anonymous reviewers.

607

608

609

610

611

612

613

614

615

616

617

618

619

620

621

622

623 Bibliography

624

625 Agrinier, P., and Cannat, M., 1997, Oxygen-isotope constraints on serpentinization processes in
626 ultramafic rocks from the Mid-Atlantic Ridge (23°N), *in* Karson, J.A., Cannat, M., Miller, D.J., and
627 Elthon, D. eds., *Proceedings of the Ocean Drilling Program, 153 Scientific Results*, Ocean Drilling
628 Program, *Proceedings of the Ocean Drilling Program*, v. 153, doi:10.2973/odp.proc.sr.153.1997.

629 Andreani, M., Mével, C., Boullier, A.-M., and Escartín, J., 2007, Dynamic control on serpentine
630 crystallization in veins: Constraints on hydration processes in oceanic peridotites: *Geochemistry,*
631 *Geophysics, Geosystems*, v. 8, p. Q02012, doi:10.1029/2006GC001373.

632 Aslanian, D. et al., 2009, Brazilian and African passive margins of the Central Segment of the South
633 Atlantic Ocean: Kinematic constraints: *Tectonophysics*, v. 468, p. 98–112,
634 doi:10.1016/j.tecto.2008.12.016.

635 Avedik, F., and Olivet, J.-L., 1994, Norgasis cruise, RV Le Nadir., <https://doi.org/10.17600/94000050>.

636 Ball, P., Eagles, G., Ebinger, C., McClay, K., and Totterdell, J., 2013, The spatial and temporal evolution of
637 strain during the separation of Australia and Antarctica: *Geochemistry, Geophysics, Geosystems*,
638 v. 14, p. 2771–2799, doi:10.1002/ggge.20160.

639 Bayrakci, G. et al., 2016, Fault-controlled hydration of the upper mantle during continental rifting:
640 *Nature Geoscience*, doi:10.1038/ngeo2671.

641 Beslier, M.O. et al., 2004, Une large transition continent-océan en pied de marge sud-ouest australienne:
642 premiers résultats de la campagne MARGAU/MD110: *Bulletin de la société Géologique de*
643 *France*, v. 175, p. 629–641.

644 Bodinier, J.L., 1988, Geochemistry and petrogenesis of the Lanzo peridotite body, western Alps:
645 *Tectonophysics*, v. 149, p. 67–88, doi:10.1016/0040-1951(88)90119-9.

646 Boillot, G., and Froitzheim, N., 2001, Non-volcanic rifted margins, continental break-up and the onset of
647 sea-floor spreading: some outstanding questions: *Geological Society, London, Special*
648 *Publications*, v. 187, p. 9–30, doi:10.1144/GSL.SP.2001.187.01.02.

649 Boillot, G., Girardeau, J., and Kornprobst, J., 1988, Rifting of the Galicia margin: crustal thinning and
650 emplacement of mantle rocks on the seafloor: *Proceedings of the Ocean Drilling Program,*
651 *Scientific Results*, v. 103, p. 741–756.

652 Boillot, G., Grimaud, S., Mauffret, A., Mougénot, D., Kornprobst, J., Mergoïl-Daniel, J., and Torrent, G.,
653 1980, Ocean-continent boundary off the Iberian margin: A serpentinite diapir west of the Galicia
654 Bank: *Earth and Planetary Science Letters*, v. 48, p. 23–34, doi:10.1016/0012-821X(80)90166-1.

655 Bonatti, E., Lawrence, J.R., and Morandi, N., 1984, Serpentinization of oceanic peridotites: temperature
656 dependence of mineralogy and boron content: *Earth and Planetary Science Letters*, v. 70, p. 88–
657 94, doi:10.1016/0012-821X(84)90211-5.

- 658 Bonatti, E., Seyler, M., Channell, J., Giraudeau, J., and Mascle, G., 1990, Peridotites drilled from the
659 Tyrrhenian sea, ODP Leg 107, *in* Kastens, K.A., Mascle, J., and et al. eds., Proceedings of the
660 Ocean Drilling Program, 107 Scientific Results, Ocean Drilling Program, Proceedings of the Ocean
661 Drilling Program, v. 107, doi:10.2973/odp.proc.sr.107.1990.
- 662 Bown, J.W., and White, R.S., 1994, Variation with spreading rate of oceanic crustal thickness and
663 geochemistry: *Earth and Planetary Science Letters*, v. 121, p. 435–449.
- 664 Buck, W.R., 1988, flexural rotation of normal faults: *Tectonics*, v. 7, p. 959–973,
665 doi:10.1029/TC007i005p00959.
- 666 Canales, J.P., Dunn, R.A., Arai, R., and Sohn, R.A., 2017, Seismic imaging of magma sills beneath an
667 ultramafic-hosted hydrothermal system: *Geology*, p. G38795.1, doi:10.1130/G38795.1.
- 668 Chian, D., Loudon, K.E., Minshull, T.A., and Whitmarsh, R.B., 1999, Deep structure of the ocean-continent
669 transition in the southern Iberia Abyssal Plain from seismic refraction profiles: *Ocean Drilling
670 Program (Legs 149 and 173) transect: Journal of Geophysical Research: Solid Earth*, v. 104, p.
671 7443–7462, doi:10.1029/1999JB900004.
- 672 Chian, D., Loudon, K.E., and Reid, I., 1995, Crustal structure of the Labrador Sea conjugate margin and
673 implications for the formation of nonvolcanic continental margins: *Journal of Geophysical
674 Research: Solid Earth*, v. 100, p. 24239–24253, doi:10.1029/95JB02162.
- 675 Cole, P.B., Minshull, T.A., and Whitmarsh, R.B., 2002, Azimuthal seismic anisotropy in a zone of exhumed
676 continental mantle, West Iberia margin: *Geophysical Journal International*, v. 151, p. 517–533,
677 doi:10.1046/j.1365-246X.2002.01781.x.
- 678 Cowie, L., Angelo, R.M., Kusznir, N.J., Manatschal, G., and Horn, B., 2015, The palaeo-bathymetry of base
679 Aptian salt deposition on the northern Angolan rifted margin: constraints from flexural back-
680 stripping and reverse post-break-up thermal subsidence modelling: *Petroleum Geoscience*, p.
681 2014– 087, doi:10.1144/petgeo2014-087.
- 682 Dean, S.M., Minshull, T.A., Whitmarsh, R.B., and Loudon, K.E., 2000, Deep structure of the ocean-
683 continent transition in the southern Iberia Abyssal Plain from seismic refraction profiles: *The
684 IAM-9 transect at 40°20'N: Journal of Geophysical Research: Solid Earth*, v. 105, p. 5859–5885,
685 doi:10.1029/1999JB900301.
- 686 Decitre, S., Deloule, E., Reisberg, L., James, R., Agrinier, P., and Mével, C., 2002, Behavior of Li and its
687 isotopes during serpentinization of oceanic peridotites: *Geochemistry, Geophysics, Geosystems*,
688 v. 3, p. 1–20, doi:10.1029/2001GC000178.
- 689 deMartin, B.J., Sohn, R.A., Canales, J.P., and Humphris, S.E., 2007, Kinematics and geometry of active
690 detachment faulting beneath the Trans-Atlantic Geotraverse (TAG) hydrothermal field on the
691 Mid-Atlantic Ridge: *Geology*, v. 35, p. 711–714, doi:10.1130/G23718A.1.
- 692 Desmurs, L., Manatschal, G., and Bernoulli, D., 2001, The Steinmann Trinity revisited: mantle exhumation
693 and magmatism along an ocean-continent transition: the Platta nappe, eastern Switzerland:
694 *Geological Society, London, Special Publications*, v. 187, p. 235–266,
695 doi:10.1144/GSL.SP.2001.187.01.12.

- 696 Desmurs, L., Müntener, O., and Manatschal, G., 2002, Onset of magmatic accretion within a magma-poor
697 rifted margin: a case study from the Platta ocean-continent transition, eastern Switzerland:
698 *Contributions to Mineralogy and Petrology*, v. 144, p. 365–382, doi:10.1007/s00410-002-0403-4.
- 699 Direen, N.G., Stagg, H.M.J., Symonds, P.A., and Colwell, J.B., 2011, Dominant symmetry of a conjugate
700 southern Australian and East Antarctic magma-poor rifted margin segment: *Geochemistry
701 Geophysics Geosystems*, v. 12, p. 29 PP., doi:201110.1029/2010GC003306.
- 702 Dunn, R.A., Arai, R., Eason, D.E., Canales, J.P., and Sohn, R.A., 2017, Three-Dimensional Seismic Structure
703 of the Mid-Atlantic Ridge: An Investigation of Tectonic, Magmatic, and Hydrothermal Processes
704 in the Rainbow Area: *Mid-Atlantic Ridge Seismic Structure: Journal of Geophysical Research:
705 Solid Earth*, v. 122, p. 9580–9602, doi:10.1002/2017JB015051.
- 706 Escartín, J., Hirth, G., and Evans, B., 1997, Nondilatant brittle deformation of serpentinites: Implications
707 for Mohr-Coulomb theory and the strength of faults: *Journal of Geophysical Research: Solid
708 Earth*, v. 102, p. 2897–2913, doi:10.1029/96JB02792.
- 709 Escartín, J., Hirth, G., and Evans, B., 2001, Strength of slightly serpentinitized peridotites: Implications for
710 the tectonics of oceanic lithosphere: *Geology*, v. 29, p. 1023–1026, doi:10.1130/0091-
711 7613(2001)029<1023:SOSSPI>2.0.CO;2.
- 712 Fumagalli, P., Borghini, G., Rampone, E., and Poli, S., 2017, Experimental calibration of Forsterite–
713 Anorthite–Ca-Tschermak–Enstatite (FACE) geobarometer for mantle peridotites: *Contributions
714 to Mineralogy and Petrology*, v. 172, p. 38, doi:10.1007/s00410-017-1352-2.
- 715 Funck, T., Hopper, J.R., Larsen, H.C., Loudon, K.E., Tucholke, B.E., and Holbrook, W.S., 2003, Crustal
716 structure of the ocean-continent transition at Flemish Cap: Seismic refraction results: *Journal of
717 Geophysical Research*, v. 108, p. 2531, doi:10.1029/2003JB002434.
- 718 Gaina, C., Müller, R.D., Brown, B., Ishihara, T., and Ivanov, S.V., 2007, Breakup and early seafloor
719 spreading between India and Antarctica: *Geophysical Journal International*, v. 170, p. 151–169,
720 doi:10.1111/j.1365-246X.2007.03450.x.
- 721 Gibbons, A.D., Whittaker, J.M., and Müller, R.D., 2013, The breakup of East Gondwana: Assimilating
722 constraints from Cretaceous ocean basins around India into a best-fit tectonic model: *Journal of
723 Geophysical Research: Solid Earth*, v. 118, p. 808–822, doi:10.1002/jgrb.50079.
- 724 Gillard, M., Autin, J., and Manatschal, G., 2016a, Fault systems at hyper-extended rifted margins and
725 embryonic oceanic crust: Structural style, evolution and relation to magma: *Marine and
726 Petroleum Geology*, v. 76, p. 51–67, doi:10.1016/j.marpetgeo.2016.05.013.
- 727 Gillard, M., Autin, J., Manatschal, G., Sauter, D., Munsch, M., and Schaming, M., 2015,
728 Tectonomagmatic evolution of the final stages of rifting along the deep conjugate Australian-
729 Antarctic magma-poor rifted margins: Constraints from seismic observations: *Tectonics*, v. 34, p.
730 2015TC003850, doi:10.1002/2015TC003850.
- 731 Gillard, M., Manatschal, G., and Autin, J., 2016b, How can asymmetric detachment faults generate
732 symmetric Ocean Continent Transitions? *Terra Nova*, v. 28, p. 27–34, doi:10.1111/ter.12183.

- 733 Gillard, M., Sauter, D., Tugend, J., Tomasi, S., Epin, M.-E., and Manatschal, G., 2017, Birth of an oceanic
734 spreading center at a magma-poor rift system: *Scientific Reports*, v. 7, p. 15072,
735 doi:10.1038/s41598-017-15522-2.
- 736 Higgle, K., and Tommasi, A., 2014, Deformation in a partially molten mantle: Constraints from plagioclase
737 lherzolites from Lanzo, western Alps: *Tectonophysics*, v. 615–616, p. 167–181,
738 doi:10.1016/j.tecto.2014.01.007.
- 739 Hölker, A.B., Manatschal, G., Holliger, K., and Bernoulli, D., 2002, Seismic structure and response of
740 ocean-continent transition zones: *Marine Geophysical Researches*, v. 23, p. 319–334.
- 741 Holtzman, B.K., and Kendall, J.-M., 2010, Organized melt, seismic anisotropy, and plate boundary
742 lubrication: *Geochemistry, Geophysics, Geosystems*, v. 11, p. Q0AB06,
743 doi:10.1029/2010GC003296.
- 744 Holtzman, B.K., Kohlstedt, D.L., Zimmerman, M.E., Heidelbach, F., Hiraga, T., and Hustoft, J., 2003, Melt
745 Segregation and Strain Partitioning: Implications for Seismic Anisotropy and Mantle Flow:
746 *Science*, v. 301, p. 1227–1230, doi:10.1126/science.1087132.
- 747 Hopper, J.R., Funck, T., Tucholke, B.E., Larsen, H.C., Holbrook, W.S., Loudon, K.E., Shillington, D., and Lau,
748 H., 2004, Continental breakup and the onset of ultraslow seafloor spreading off Flemish Cap on
749 the Newfoundland rifted margin: *Geology*, v. 32, p. 93–96, doi:10.1130/G19694.1.
- 750 Hopper, J.R., Funck, T., Tucholke, B.E., Loudon, K.E., Holbrook, W.S., and Christian Larsen, H., 2006, A
751 deep seismic investigation of the Flemish Cap margin: implications for the origin of deep
752 reflectivity and evidence for asymmetric break-up between Newfoundland and Iberia:
753 *Geophysical Journal International*, v. 164, p. 501–515, doi:10.1111/j.1365-246X.2006.02800.x.
- 754 Kaczmarek, M.-A., and Müntener, O., 2008, Juxtaposition of Melt Impregnation and High-Temperature
755 Shear Zones in the Upper Mantle; Field and Petrological Constraints from the Lanzo Peridotite
756 (Northern Italy): *Journal of Petrology*, v. 49, p. 2187–2220, doi:10.1093/petrology/egn065.
- 757 Kaczmarek, M.-A., and Müntener, O., 2010, The variability of peridotite composition across a mantle
758 shear zone (Lanzo massif, Italy): interplay of melt focusing and deformation: *Contributions to
759 Mineralogy and Petrology*, v. 160, p. 663–679, doi:10.1007/s00410-010-0500-8.
- 760 Kaczmarek, M.-A., and Tommasi, A., 2011, Anatomy of an extensional shear zone in the mantle, Lanzo
761 massif, Italy: *Geochemistry, Geophysics, Geosystems*, v. 12, doi:10.1029/2011GC003627.
- 762 Keen, C.E., Dickie, K., and Dafoe, L.T., 2017, Structural characteristics of the ocean-continent transition
763 along the rifted continental margin, offshore central Labrador: *Marine and Petroleum Geology*,
764 doi:10.1016/j.marpetgeo.2017.10.012.
- 765 Keen, C.E., Potter, P., and Srivastava, S.P., 1994, Deep seismic reflection data across the conjugate
766 margins of the Labrador Sea: *Canadian Journal of Earth Sciences*, v. 31, p. 192–205,
767 doi:10.1139/e94-016.

- 768 Kohlstedt, D.L., and Holtzman, B.K., 2009, Shearing Melt Out of the Earth: An Experimentalist's
769 Perspective on the Influence of Deformation on Melt Extraction: *Annual Review of Earth and*
770 *Planetary Sciences*, v. 37, p. 561–593, doi:10.1146/annurev.earth.031208.100104.
- 771 Lemoine, M., Tricart, P., and Boillot, G., 1987, Ultramafic and gabbroic ocean floor of the Ligurian Tethys
772 (Alps, Corsica, Apennines): In search of a genetic imodel: *Geology*, v. 15, p. 622–625,
773 doi:10.1130/0091-7613(1987)15<622:UAGOFO>2.0.CO;2.
- 774 Linckens, J., Herwegh, M., Müntener, O., and Mercolli, I., 2011, Evolution of a polymineralic mantle shear
775 zone and the role of second phases in the localization of deformation: *Journal of Geophysical*
776 *Research*, v. 116, doi:10.1029/2010JB008119.
- 777 Lymer, G., Cresswell, D.J.F., Reston, T.J., Bull, J.M., Sawyer, D.S., Morgan, J.K., Stevenson, C., Causer, A.,
778 Minshull, T.A., and Shillington, D.J., 2019, 3D development of detachment faulting during
779 continental breakup: *Earth and Planetary Science Letters*, v. 515, p. 90–99,
780 doi:10.1016/j.epsl.2019.03.018.
- 781 Maffione, M., Morris, A., Plümpner, O., and van Hinsbergen, D.J.J., 2014, Magnetic properties of variably
782 serpentinized peridotites and their implication for the evolution of oceanic core complexes:
783 *Geochemistry, Geophysics, Geosystems*, v. 15, doi:10.1002/2013GC004993.
- 784 Manatschal, G., Sauter, D., Karpoff, A.M., Masini, E., Mohn, G., and Lagabriele, Y., 2011, The Chenaillet
785 Ophiolite in the French/Italian Alps: An ancient analogue for an Oceanic Core Complex? *Lithos*, v.
786 124, p. 169–184, doi:10.1016/j.lithos.2010.10.017.
- 787 Mével, C., 2003, Serpentinization of abyssal peridotites at mid-ocean ridges: *Comptes Rendus*
788 *Geoscience*, v. 335, p. 825–852, doi:10.1016/j.crte.2003.08.006.
- 789 Mevel, C., Caby, R., and Kienast, J.-R., 1978, Amphibolite facies conditions in the oceanic crust: example
790 of amphibolitized flaser-gabbro and amphibolites from the Chenaillet ophiolite massif (Hautes
791 Alpes, France): *Earth and Planetary Science Letters*, v. 39, p. 98–108, doi:10.1016/0012-
792 821X(78)90146-2.
- 793 Miller, D.J., and Christensen, N.I. 25. SEISMIC VELOCITIES OF LOWER CRUSTAL AND UPPER MANTLE
794 ROCKS FROM THE SLOW-SPREADING MID-ATLANTIC RIDGE, SOUTH OF THE KANE TRANSFORM
795 ZONE (MARK);, [http://www-](http://www-odp.tamu.edu/publications/153_SR/VOLUME/CHAPTERS/sr153_25.pdf)
796 [odp.tamu.edu/publications/153_SR/VOLUME/CHAPTERS/sr153_25.pdf](http://www-odp.tamu.edu/publications/153_SR/VOLUME/CHAPTERS/sr153_25.pdf) (accessed June 2014).
- 797 Minshull, T.A., 2009, Geophysical characterisation of the ocean–continent transition at magma-poor
798 rifted margins: *Comptes Rendus Geoscience*, v. 341, p. 382–393, doi:10.1016/j.crte.2008.09.003.
- 799 Minshull, T.A., Dean, S.M., and Whitmarsh, R.B., 2014, The peridotite ridge province in the southern
800 Iberia Abyssal Plain: Seismic constraints revisited: *Journal of Geophysical Research: Solid Earth*,
801 p. 2014JB011011, doi:10.1002/2014JB011011.
- 802 Minshull, T.A., Muller, M.R., Robinson, C.J., White, R.S., and Bickle, M.J., 1998, Is the oceanic Moho a
803 serpentinization front? *Geological Society, London, Special Publications*, v. 148, p. 71–80,
804 doi:10.1144/GSL.SP.1998.148.01.05.

- 805 Momoh, E., Cannat, M., Watremez, L., Leroy, S., and Singh, S.C., 2017, Quasi-3-D Seismic Reflection
806 Imaging and Wide-Angle Velocity Structure of Nearly Amagmatic Oceanic Lithosphere at the
807 Ultraslow-Spreading Southwest Indian Ridge: *Journal of Geophysical Research: Solid Earth*, v.
808 122, p. 2017JB014754, doi:10.1002/2017JB014754.
- 809 Montadert, L., Roberts, D.G., de Charpal, O., and Guennoc, P., 1979, Rifting and subsidence of the
810 northern continental margin of the bay of biscay: *Ocean Drilling Program : College Station*,
811 http://www.deepseadrilling.org/48/volume/dsdp48_54.pdf (accessed July 2014).
- 812 Morgan, J.P., and Chen, Y.J., 1993, The genesis of oceanic crust: Magma injection, hydrothermal
813 circulation, and crustal flow: *Journal of Geophysical Research: Solid Earth*, v. 98, p. 6283–6297,
814 doi:10.1029/92JB02650.
- 815 Muntener, O., Manatschal, G., Desmurs, L., and Pettke, T., 2010, Plagioclase Peridotites in Ocean-
816 Continent Transitions: Refertilized Mantle Domains Generated by Melt Stagnation in the Shallow
817 Mantle Lithosphere: *Journal of Petrology*, v. 51, p. 255–294, doi:10.1093/petrology/egp087.
- 818 Müntener, O., Pettke, T., Desmurs, L., Meier, M., and Schaltegger, U., 2004, Refertilization of mantle
819 peridotite in embryonic ocean basins: trace element and Nd isotopic evidence and implications
820 for crust–mantle relationships: *Earth and Planetary Science Letters*, v. 221, p. 293–308,
821 doi:10.1016/S0012-821X(04)00073-1.
- 822 Müntener, O., and Piccardo, G.B., 2003, Melt migration in ophiolitic peridotites: the message from
823 Alpine-Apennine peridotites and implications for embryonic ocean basins: *Geological Society*,
824 London, Special Publications, v. 218, p. 69–89, doi:10.1144/GSL.SP.2003.218.01.05.
- 825 Nemcok, M., Sinha, S.T., Stuart, C.J., Welker, C., Choudhuri, M., Sharma, S.P., Misra, A.A., Sinha, N., and
826 Venkatraman, S., 2013, East Indian margin evolution and crustal architecture: integration of
827 deep reflection seismic interpretation and gravity modelling: *Geological Society, London, Special*
828 *Publications*, v. 369, p. 477–496, doi:10.1144/SP369.6.
- 829 Nicolas, A., Bouchez, J.L., and Boudier, F., 1972, Interpretation cinématique des déformations plastiques
830 dans le massif de Lherzolite de Ianzo (Alpes piémontaises) — comparaison avec d’autres Massifs:
831 *Tectonophysics*, v. 14, p. 143–171, doi:10.1016/0040-1951(72)90107-2.
- 832 Niida, K., and Green, D.H., 1999, Stability and chemical composition of pargasitic amphibole in MORB
833 pyrolite under upper mantle conditions: *Contributions to Mineralogy and Petrology*, v. 135, p.
834 18–40, doi:10.1007/s004100050495.
- 835 Nirrengarten, M., Manatschal, G., Tugend, J., Kuszniir, N., and Sauter, D., 2018, Kinematic Evolution of the
836 Southern North Atlantic: Implications for the Formation of Hyperextended Rift Systems:
837 *Tectonics*, p. 2017TC004495, doi:10.1002/2017TC004495.
- 838 Nirrengarten, M., Manatschal, G., Yuan, X.P., Kuszniir, N.J., and Maillot, B., 2016, Application of the
839 critical Coulomb wedge theory to hyper-extended, magma-poor rifted margins: *Earth and*
840 *Planetary Science Letters*, v. 442, p. 121–132, doi:10.1016/j.epsl.2016.03.004.
- 841 Oakey, G.N., and Chalmers, J.A., 2012, A new model for the Paleogene motion of Greenland relative to
842 North America: Plate reconstructions of the Davis Strait and Nares Strait regions between

843 Canada and Greenland: *Journal of Geophysical Research: Solid Earth*, v. 117,
844 doi:10.1029/2011JB008942.

845 O'Hanley, D.S., 1996, *Serpentinites: records of tectonic and petrological history*: New York, Oxford
846 University Press, Oxford monographs on geology and geophysics no. 34, 277 p.

847 Pérez-Gussinyé, M., and Reston, T.J., 2001, Rheological evolution during extension at nonvolcanic rifted
848 margins: Onset of serpentinization and development of detachments leading to continental
849 breakup: *Journal of Geophysical Research: Solid Earth*, v. 106, p. 3961–3975,
850 doi:10.1029/2000JB900325.

851 Pérez-Gussinyé, M., Reston, T.J., and Morgan, J.P., 2001, Serpentinization and magmatism during
852 extension at non-volcanic margins: the effect of initial lithospheric structure: Geological Society,
853 London, Special Publications, v. 187, p. 551–576, doi:10.1144/GSL.SP.2001.187.01.27.

854 Peron-Pinvidic, G., Manatschal, G., and Osmundsen, P.T., 2013, Structural comparison of archetypal
855 Atlantic rifted margins: A review of observations and concepts: *Marine and Petroleum Geology*,
856 v. 43, p. 21–47, doi:10.1016/j.marpetgeo.2013.02.002.

857 Peron-Pinvidic, G., and Osmundsen, P.T., 2016, Architecture of the distal and outer domains of the Mid-
858 Norwegian rifted margin: Insights from the Rån-Gjallar ridges system: *Marine and Petroleum
859 Geology*, v. 77, p. 280–299, doi:10.1016/j.marpetgeo.2016.06.014.

860 Peron-Pinvidic, G., Osmundsen, P.T., and Ebbing, J., 2016, Mismatch of geophysical datasets in distal
861 rifted margin studies: *Terra Nova*, v. 28, p. 340–347, doi:10.1111/ter.12226.

862 Picazo, S., Müntener, O., Manatschal, G., Bauville, A., Karner, G., and Johnson, C., 2016, Mapping the
863 nature of mantle domains in Western and Central Europe based on clinopyroxene and spinel
864 chemistry: Evidence for mantle modification during an extensional cycle: *Lithos*, v. 266–267, p.
865 233–263, doi:10.1016/j.lithos.2016.08.029.

866 Piccardo, G.B., Zanetti, A., and Müntener, O., 2007, Melt/peridotite interaction in the Southern Lanzo
867 peridotite: Field, textural and geochemical evidence: *Lithos*, v. 94, p. 181–209,
868 doi:10.1016/j.lithos.2006.07.002.

869 Pickup, S.L.B., Whitmarsh, R.B., Fowler, C.M.R., and Reston, T.J., 1996, Insight into the nature of the
870 ocean-continent transition off West Iberia from a deep multichannel seismic reflection profile:
871 *Geology*, v. 24, p. 1079–1082, doi:10.1130/0091-7613(1996)024<1079:IITNOT>2.3.CO;2.

872 Ranero, C.R., and Pérez-Gussinyé, M., 2010, Sequential faulting explains the asymmetry and extension
873 discrepancy of conjugate margins: *Nature*, v. 468, p. 294–299, doi:10.1038/nature09520.

874 Reston, T., 2007, Extension discrepancy at North Atlantic nonvolcanic rifted margins: Depth-dependent
875 stretching or unrecognized faulting? *Geology*, v. 35, p. 367–370, doi:10.1130/G23213A.1.

876 Reston, T.J., 1996, The S reflector west of Galicia: the seismic signature of a detachment fault:
877 *Geophysical Journal International*, v. 127, p. 230–244, doi:10.1111/j.1365-246X.1996.tb01547.x.

- 878 Reston, T.J., 2009, The structure, evolution and symmetry of the magma-poor rifted margins of the North
879 and Central Atlantic: A synthesis: *Tectonophysics*, v. 468, p. 6–27,
880 doi:10.1016/j.tecto.2008.09.002.
- 881 Reston, T.J., Leythaeuser, T., Booth-Rea, G., Sawyer, D., Klaeschen, D., and Long, C., 2007, Movement
882 along a low-angle normal fault: The S reflector west of Spain: *Geochemistry, Geophysics,*
883 *Geosystems*, v. 8, p. Q06002, doi:10.1029/2006GC001437.
- 884 Reston, T.J., and McDermott, K.G., 2011, Successive Detachment Faults and Mantle Unroofing at
885 Magma-Poor Rifted Margins: *Geology*, v. 39, p. 1071–1074, doi:10.1130/G32428.1.
- 886 Reston, T.J., and Pérez-Gussinyé, M., 2007, Lithospheric extension from rifting to continental breakup at
887 magma-poor margins: rheology, serpentinisation and symmetry: *International Journal of Earth*
888 *Sciences*, v. 96, p. 1033–1046, doi:10.1007/s00531-006-0161-z.
- 889 Reston, T.J., and Ranero, C.R., 2011, The 3-D geometry of detachment faulting at mid-ocean ridges:
890 *Geochemistry, Geophysics, Geosystems*, v. 12, p. Q0AG05, doi:10.1029/2011GC003666.
- 891 Ryan, M.P., 1993, Neutral buoyancy and the structure of mid-ocean ridge magma reservoirs: *Journal of*
892 *Geophysical Research: Solid Earth*, v. 98, p. 22321–22338, doi:10.1029/93JB02394.
- 893 Sanfilippo, A., and Tribuzio, R., 2011, Melt transport and deformation history in a nonvolcanic ophiolitic
894 section, northern Apennines, Italy: Implications for crustal accretion at slow spreading settings:
895 *Geochemistry, Geophysics, Geosystems*, v. 12, p. n/a-n/a.
- 896 Sauter, D. et al., 2013, Continuous exhumation of mantle-derived rocks at the Southwest Indian Ridge for
897 11 million years: *Nature Geoscience*, v. 6, p. 314–320, doi:10.1038/ngeo1771.
- 898 Sauter, D., Tugend, J., Gillard, M., Nirrengarten, M., Autin, J., Manatschal, G., Cannat, M., Leroy, S., and
899 Schaming, M., 2018, Oceanic basement roughness alongside magma-poor rifted margins: insight
900 into initial seafloor spreading: *Geophysical Journal International*, v. 212, p. 900–915,
901 doi:10.1093/gji/ggx439.
- 902 Sawyer, D.S., Whitmarsh, R.B., and Klaus, A., 1994, *Proceedings of the Ocean Drilling Program, Initial*
903 *Reports*, v. 149, doi:doi:10.2973/odp.proc.ir.149.1994.
- 904 Sayers, J., Symonds, P.A., Direen, N.G., and Bernardel, G., 2001, Nature of the continent-ocean transition
905 on the non-volcanic rifted margin of the central Great Australian Bight: *Geological Society,*
906 *London, Special Publications*, v. 187, p. 51–76, doi:10.1144/GSL.SP.2001.187.01.04.
- 907 Schuba, C.N., Gray, G.G., Morgan, J.K., Sawyer, D.S., Shillington, D.J., Reston, T.J., Bull, J.M., and Jordan,
908 B.E., 2018, A low-angle detachment fault revealed: Three-dimensional images of the S-reflector
909 fault zone along the Galicia passive margin: *Earth and Planetary Science Letters*, v. 492, p. 232–
910 238, doi:10.1016/j.epsl.2018.04.012.
- 911 Sibuet, J.-C., 1992, New constraints on the formation of the non-volcanic continental Galicia–Flemish Cap
912 conjugate margins: *Journal of the Geological Society*, v. 149, p. 829–840,
913 doi:10.1144/gsjgs.149.5.0829.

- 914 Sibuet, J.-C., and Tucholke, B.E., 2012, The geodynamic province of transitional lithosphere adjacent to
915 magma-poor continental margins: Geological Society, London, Special Publications, v. 369, p.
916 SP369.15, doi:10.1144/SP369.15.
- 917 Sparks, D.W., and Parmentier, E.M., 1994, The Generation and Migration of Partial Melt beneath Oceanic
918 Spreading Centers, *in* Magmatic Systems, M. P. Ryan, International Geophysics Series, v. 57, p.
919 55–76.
- 920 Stagg, H.M.J., Colwel, J.B., Direen, N.G., O'Brien, P.E., Bernardel, G., Borissova, I., Brown, B.J., and
921 Ishirara, T., 2004, Geology of the Continental Margin of Enderby and Mac. Robertson Lands, East
922 Antarctica: Insights from a Regional Data Set: Marine Geophysical Researches, v. 25, p. 183–219,
923 doi:10.1007/s11001-005-1316-1.
- 924 Stagg, H., and Schiwy, S., 2002, Marine geophysical surveys completed off Antarctica: AusGeo News 66,
925 p. 18–19.
- 926 Thinon, I., Matias, L., Réhault, J.-P., Hirn, A., Fidalgo-González, L., and Avedik, F., 2003, Deep structure of
927 the Armorican Basin (Bay of Biscay): a review of Norgasis seismic reflection and refraction data:
928 Journal of the Geological Society of London, v. 160, p. 99–116, doi:10.1144/0016-764901-103.
- 929 Totterdell, J.M., Blevin, J.E., Struckmeyer, H.I.M., Bradshaw, B.E., Colwell, J.B., and Kennard, J.M., 2000, A
930 new sequence framework for the Great Australian Bight: starting with a clean slate.: APPEA
931 Journal, p. 95–117.
- 932 Tribuzio, R., Riccardi, M.P., and Ottolini, L., 1995, Trace element redistribution in high-temperature
933 deformed gabbros from East Ligurian ophiolites (Northern Apennines, Italy): constraints on the
934 origin of syndeformation fluids: Journal of Metamorphic Geology, v. 13, p. 367–377,
935 doi:10.1111/j.1525-1314.1995.tb00226.x.
- 936 Tucholke, B.E., Sibuet, J.C., and Klaus, A., 2004, Proceedings of the Ocean Drilling Program, Initial
937 Reports, Volume 210, *in* v. 210.
- 938 Tucholke, B.E., Sawyer, D.S., and Sibuet, J.-C., 2007, Breakup of the Newfoundland–Iberia rift: Geological
939 Society, London, Special Publications, v. 282, p. 9–46, doi:10.1144/SP282.2.
- 940 Tucholke, B.E., Behn, M.D., Buck, W.R., and Lin, J., 2008, Role of melt supply in oceanic detachment
941 faulting and formation of megamullions: Geology, v. 36, p. 455–458, doi:10.1130/G24639A.1.
- 942 Tugend, J., Gillard, M., Manatschal, G., Nirrengarten, M., Harkin, C., Epin, M.-E., Sauter, D., Autin, J.,
943 Kuszniir, N., and McDermott, K., 2018, Reappraisal of the magma-rich versus magma-poor rifted
944 margin archetypes: Geological Society, London, Special Publications, p. SP476.9,
945 doi:10.1144/SP476.9.
- 946 Tugend, J., Manatschal, G., and Kuszniir, N.J., 2015, Spatial and temporal evolution of hyperextended rift
947 systems: Implication for the nature, kinematics, and timing of the Iberian-European plate
948 boundary: Geology, v. 43, p. 15–18, doi:10.1130/G36072.1.

- 949 Tugend, J., Manatschal, G., Kuszniir, N.J., Masini, E., Mohn, G., and Thinon, I., 2014, Formation and
950 deformation of hyperextended rift systems: Insights from rift domain mapping in the Bay of
951 Biscay-Pyrenees: *Tectonics*, v. 33, p. 2014TC003529, doi:10.1002/2014TC003529.
- 952 Ulmer, P., and Trommsdorf, V., 1999, Phase relations of hydrous mantle subducting to 300 km, *in* Fei, Y.,
953 Bertka, C., and Mysen eds., *Mantle Petrology: Field observations and High Pressure*
954 *Experimentation*, The Geochemical Society, Special Publication 6, p. 24.
- 955 Ulmer, P., and Trommsdorff, V., 1995, Serpentine Stability to Mantle Depths and Subduction-Related
956 Magmatism: *Science*, v. 268, p. 858–861, doi:10.1126/science.268.5212.858.
- 957 Wernicke, B., 1981, Low-angle normal faults in the Basin and Range Province: nappe tectonics in an
958 extending orogen: *Nature*, v. 291, p. 645–648, doi:10.1038/291645a0.
- 959 White, R.S., McKenzie, D., and O’Nions, R.K., 1992, Oceanic crustal thickness from seismic measurements
960 and rare earth element inversions: *Journal of Geophysical Research: Solid Earth*, v. 97, p. 19683–
961 19715, doi:10.1029/92JB01749.
- 962 Whitmarsh, R.B., Beslier, M.O., and Wallace, P.J., 1998, Proceedings of the Ocean Drilling Program, Leg
963 173: *Proc. ODP, Init. Repts*, v. 173, p. 7–23.
- 964 Whitmarsh, R.B., White, R.S., Horsefield, S.J., Sibuet, J.-C., Recq, M., and Louvel, V., 1996, The ocean-
965 continent boundary off the western continental margin of Iberia: Crustal structure west of
966 Galicia Bank: *Journal of Geophysical Research: Solid Earth*, v. 101, p. 28291–28314,
967 doi:10.1029/96JB02579.
- 968 Williams, S.E., Whittaker, J.M., Halpin, J.A., and Müller, R.D., 2019, Australian-Antarctic breakup and
969 seafloor spreading: Balancing geological and geophysical constraints: *Earth-Science Reviews*, v.
970 188, p. 41–58, doi:10.1016/j.earscirev.2018.10.011.
- 971